KeAi
CHINESE ROOTS
GLOBAL IMPACT

Contents lists available at ScienceDirect

Petroleum Science

journal homepage: www.keaipublishing.com/en/journals/petroleum-science



Original Paper

Multi-phase deformation and analogue modelling of the Junggar Basin, NW China



Jing-Qi Zhang ^a, Fu-Sheng Yu ^{a, b, *}, Yue-Feng Wang ^a, Zhuo-Yi Shen ^a, Jin-Lei Xiu ^c, Yan Xue ^c. Long-Fei Shao ^a

- ^a College of Geosciences, China University of Petroleum, Beijing, 102249, China
- ^b State Key Laboratory of Petroleum Resources and Processing, China University of Petroleum, Beijing, 102249, China
- ^c Research Institute of Exploration and Development, Shengli Oilfield Company, SINOPEC, Dongying, 257000, Shandong, China

ARTICLE INFO

Article history: Received 31 January 2024 Received in revised form 22 May 2024 Accepted 25 June 2024 Available online 27 June 2024

Edited by Jie Hao

Keywords: Multi-phase deformation Analogue modelling Tectonic evolution Deformation characteristics Junggar basin

ABSTRACT

Based on the theory of superimposed deformation and the regional tectonic background, the multi-phase non-coaxial superimposed structures in Junggar Basin were systematically analyzed using seismic interpretation, field outcrop observation, and paleo-stress field recovery methods according to the characteristics of the current tectonic framework. Moreover, the tectonic evolution process of the basin was reconstructed using sandbox analogue modelling technology. The results showed that the study area has experienced five phases of non-coaxial deformation with superimposition: The first phase of deformation (D₁) is characterized by NNE-SSW extension during late Carboniferous to early Permian, which formed large graben, half graben and other extensional structure style around the basin. The second phase of deformation (D2) is represented by NE-SW compression during the middle to late Permian, and it comprised numerous contraction structures that developed based on D₁. The basic form of the entire basin is alternating uplift and depression. The third phase of deformation (D₃) is the NW-SE transpressional strike-slip in the Triassic-Jurassic, which produced numerous strike-slip structural styles in the middle part of the basin. The fourth phase of deformation (D₄) is the uniform sedimentation during Cretaceous, and the fifth phase (D₅) is the compression along NNE-SSW due to the North Tianshan northward thrust, which produced three rows of fold thrust belts and tear faults in the front of the mountain in the southern margin of the basin. The newly established three-dimensional tectonic evolution model shows that, based on the large number of NW-trending grabens and half grabens in the Carboniferous basement of Junggar Basin, multiple level NE trending uplifts have formed with the joint superposition of the late structural inversion and multiple stress fields. This has resulted in the current tectonic units of alternating uplifts and depressions in different directions in the study area.

© 2024 The Authors. Publishing services by Elsevier B.V. on behalf of KeAi Communications Co. Ltd. This is an open access article under the CC BY-NC-ND license (http://creativecommons.org/licenses/by-nc-nd/

4.0/).

1. Introduction

As one of the largest petroliferous basins in the northwestern part of mainland China, with its onshore hydrocarbon reserves exceeding 10.3 billion tons, it has undergone over 70 years of exploration and development. However, the comprehensive proven reserves of oil and gas in the basin are only 26.6%. Thus, it remains in the early-middle stage of exploration, indicating significant

E-mail address: fushengyu@cup.edu.cn (F.-S. Yu).

untapped potential for oil and gas resources as well as exploration and development opportunities. As the Junggar Basin has experienced long-term tectonic evolution and complicated hydrocarbon accumulation process, it is of great practical significance to deepen the basin structural characteristics and oil and gas distribution patterns under the background of multi-phase stacking and reconstruction for strengthening the national deep oil and gas exploration and development efforts (He et al., 2019; Wang et al., 2021).

The unique geological position, complicated tectonic evolution, and abundant hydrocarbon resources render the Junggar Basin an ideal area for conducting research on paleo-continental reconstruction, intracontinental evolution, active seismicity, intracontinental

^{*} Corresponding author. College of Geosciences, China University of Petroleum, Beijing, 102249, China.

dynamics, and the intricate interplay between basin structure, sedimentation, and hydrocarbon accumulation. Geologists have recognized that the Junggar Basin is a multi-phase superimposed basin (Pang, 2010; He et al., 2010, 2022; Hu et al., 2020), having undergone several tectonic changes, and was frozen in the last tectonic movement. However, due to the strong modification of prototype basins and different data or evidence, researchers still have different opinions on the evolution division of the Junggar Basin (Zhao, 1992; Zhang et al., 1998; Lai et al., 1999; Chen et al., 2002; Wu et al., 2005; Fang et al., 2006; Qu et al., 2009; He et al., 2018; Wang et al., 2022). Zhao (1992) firstly classified the basin evolution into four phases: the Permian as the rifting phase, the Triassic as the rifting-depression phase, the Jurassic to Paleogene as the depression phase, and the Neogene onwards as the uplift and subsidence phase. Zhang et al. (1998) believed that the Late Carboniferous to Permian was the development stage of the collision foreland depression, Triassic to Jurassic was the inheritance and development stage of the foreland depression in the revival period of the ancient orogenic belt, Cretaceous to Paleogene was the balanced subsidence stage of the Tianshan piedmont unified foreland depression, and the Tianshan piedmont unified foreland basin was strongly subsidence since Neogene. Based on the structure-layers and the progress of the basin research, Chen et al. (2002) defined that the terrain passed through three stages and came into being the Junggar Basin: the terrane evolution, the oceanic thrust consumption and the accretion and collage of the terrain and plates. Thus, they divided the formation and evolution of the basin into six stages. Using the foreland basin theory and with the background of evolutionary dynamics, Wu et al. (2005) divided the Junggar Basin into five evolutionary stages: collision-basin forming stage, pressure flexure stage, flexuredepression stage, depression-sedimentation stage, and foreland basin regeneration stage. Based on the deep boreholes and highresolution reflection data within the Junggar Basin, He et al. (2018) analyzed the tectonic-stratigraphic sequence and tectonic events in the periphery of the basin and indicated that the basin has undergone six evolutionary stages, which can be grouped into four nonisochronous extension-compression cycles. It is generally believed that the formation and evolution of basins from Neogene to Quaternary are related to the uplift of the Tianshan Mountain, while the primary disagreement in the division lies in the understanding of crucial periods of basin-mountain coupling in the Junggar Basin, particularly the Late Carboniferous to Permian period regarding the nature of the basin. A correct understanding of the structural evolution of the Junggar Basin contributes to identifying the macroscopic control of multi-stage structural superposition and modification on the distribution of oil and gas reservoirs in the study area.

Analogue modelling experiments have been extensively employed as an intuitive and efficient research tool to study the tectonic evolution, sedimentary evolution, and fault sealing in different margins of the Junggar Basin (He et al., 2008; Yu et al., 2009; Ding et al., 2011; Zhang et al., 2020; Shen et al., 2022; Zhang et al., 2024). Yang et al. (2003) utilized a three-dimensional numerical simulation program based on the finite element method to present the simulation of paleo-tectonic stress field in Junggar Basin during Yanshan movement. Their study demonstrated that the high values of maximum principal stress in this period were primarily located around the basin periphery, with shear stresses distributed predominantly in these areas. The minimum principal stress exhibited a belt-like distribution, generally aligning with the orientation of faults. Combining petroleum geological data and the migration capability of hydrocarbons, this stress distribution pattern facilitates the accumulation of oil and gas in relatively lowstress areas surrounded by the central uplift zone, the piedmont of the North Tianshan Mountains, and the low-stress zones in the

west, as well as high-stress areas. Wang et al. (2011) used the finite element numerical simulation method to study the paleo-stress field of the Junggar Basin at the end of Paleozoic. They determined the direction of maximum principal stress in the Late Permian Junggar region to be NW-SE, approximately at 295°, based on the study of dike swarms in the west of the basin, the simulation comparisons indicated that by the end of the Late Permian, the Junggar Basin might have been subjected to a composite effect of tenso-shear and compresso-shear mechanisms. Wang et al. (2015) utilized physical simulation experiments to investigate the deformation characteristics and tectonic evolution of Zaire Mountain, focusing on two stages of thrust-nappe structures during Carboniferous to Permian, and thrust-torsion during Triassic to Jurassic, which confirmed the presence of a thrust-shear structural system at the northwestern margin of the Junggar Basin, Zhang et al. (2024) reproduced the tectonic evolution of the Yongjin Area in the central Junggar Basin through structural physical simulation. Their study identified three sets of strike-slip fault systems by detailed interpretation of seismic data, oriented nearly E-W, NW-SE, and NE-SW within the Triassic to Jurassic strata in the study area. Through sandbox comparative experiments, they proposed that the distributed strike-slip fault system in the central Junggar Basin is controlled by both pre-existing structures and stratum properties.

Tectonic and evolutionary characteristics play an important role in controlling the generation, migration, and reservoir formation of hydrocarbons. Understanding the dynamic interplay between tectonic events and hydrocarbon accumulation is crucial for effective exploration and exploitation of petroleum resources. Based on the clarification of the deformation characteristics of each period in the region, this study reproduced the evolutionary history of multiphase tectonic superposition and modification in the study area using analogue modelling experiments and established a three-dimensional (3D) tectonic evolution model using horizontal and cross-sectional slices. The study results not only contribute to the restoration of prototype basins of each period in the region, exploring key issues in the transformation of dynamics systems of paleo-stress field, but also provide an important reference for evaluating hydrocarbon resources in complex tectonic areas.

2. Geological setting

Junggar Basin is located in the northwest of China, and it is an essential component of the spatial pattern system "three mountains and two basins" in Xinjiang (Fig. 1(a)). The entire basin appears an irregular triangular shape, with an area of about $1.36 \times 10^5 \text{ km}^2$. It has undergone multiple tectonic movements and evolutionary processes (Li et al., 2015), including the Hercynian, Indosinian, Yanshan, and Himalayan orogenesis. In terms of tectonic position, the Junggar Block is situated at the intersection of the Kazakhstan, Siberian, and Tarim ancient plates, and usually belongs to the Kazakhstan-Junggar plate according to the plate tectonic theory (Xiao et al., 1992). From a north-south perspective, it is sandwiched between the Siberian Plate and the Tarim Plate, constituting a triangular region of active continental margin plates, belonging to the convergent zone of the Late Paleozoic (He et al., 2018). The various tectonic movements, such as the Siberian Plate underwent southward accretion, or the collision between the Eurasian Plate and the Indian Plate, even the plate A-type subduction, have exerted varying degrees of influence on the tectonic evolution of this region. As a large-scale Late Paleozoic to Cenozoic continental superimposed basin, the present-day Junggar Basin is bounded by a series of thrust faults and peripheral mountain ranges, with several foreland basins in different margins (Zhou et al., 2023).

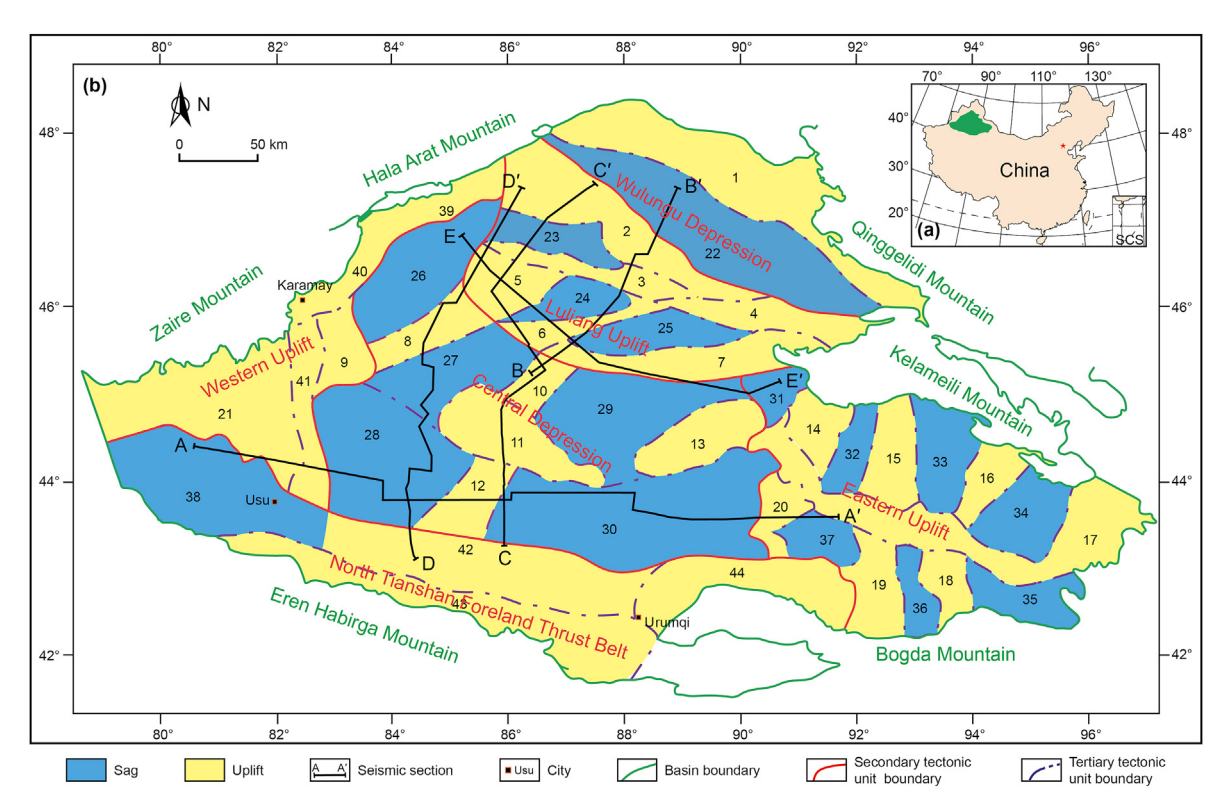


Fig. 1. Tectonic map of China showing the location of the Junggar Basin (a); tectonic units of the Junggar Basin and its adjacent regions (b). 1—Hongyan Fault Zone; 2—Shiyingtan Uplift; 3—Sangequan Uplift; 4—Dibei Uplift; 5—Xiayan Uplift; 6—Shixi Uplift; 7—Dinan Uplift; 8—Dabasong Uplift; 9—Zhongguai Uplift; 10—Mobei Uplift; 11—Mosuowan Uplift; 12—Monan Uplift; 13—Baijiahai Uplift; 14—Shazhang Uplift; 15—Huangcaohu Uplift; 16—Heishan Uplift; 17—Shaqi Uplift; 18—Gudong Uplift; 19—Guxi Uplift; 20—Beisantai Uplift; 21—Chepaizi Uplift; 22—Suosuoquan Sag; 23—Yingxi Sag; 24—Sannan Sag; 25—Dishuiquan Sag; 26—Mahu Sag; 27—Pen1Wellxi Sag; 28—Shawan Sag; 29—Dongdaohaizi Sag; 31—Wucaiwan Sag; 32—Shishugou Sag; 33—Shiqiantan Sag; 34—Wutongwozi Sag; 35—Mulei Sag; 36—Gucheng Sag; 37—Jimusar Sag; 38—Sikeshu Sag; 39—Wuxia Fault Zone; 40—Kebai Fault Zone; 41—Hongche Fault Zone; 42—Huo-Ma-Tu Anticline Belt; 43—Qigu Fault-fold Belt; 44—Fukang Fault Zone.

Based on the tectonic patterns of the basement uplift and depression of the Junggar Basin, the properties of the boundary, the types of sedimentary cover construction and evolution, the deformation characteristics of deep and shallow tectonic layers, and the control of regional fractures on stratigraphic deposition, the entire basin can be divided into six secondary tectonic units and forty-four tertiary tectonic units (Fig. 1(b)). The main secondary tectonic units include Wulungu Depression, Luliang Uplift, Central Depression, Western Uplift, Eastern Uplift and North Tianshan Foreland Thrust Belt, characterized by a structural pattern of alternating uplifts and depressions. The strike of an uplift or depression is parallel to the strike of an adjacent orogenic belt (in most areas) or intersects vertically (in eastern areas).

According to drilling data and 1:500000 regional geological map data of Xinjiang, the exposed sedimentary strata around the Junggar Basin can be divided into three regions: northwest, northeast and south margin, with slightly different lithologic combination. The stratigraphic sequence developed from the bottom to top during the Carboniferous, Permian, Triassic, Jurassic, Cretaceous, Paleogene, Neogene, and Ouaternary (Fig. 2), and it is characterized by a complete stratigraphic sequence, deep burial, and large sedimentary thickness. There are numerous discontinuities in the uplifts or sloping areas of the basin, with over ten regional unconformities developed (He et al., 2018). At the basin scale, the Triassic, Jurassic, and Cretaceous sequences are generally distributed throughout the entire basin area and can be directly tracked and compared through seismic stratigraphy. The Paleogene, Neogene and Quaternary sequences are primarily distributed in the southern part of the basin, thinning significantly towards the north. Conversely, the Carboniferous and Permian sequences are mainly

located within the basin's depressions, characterized by pronounced faulting, resulting in discontinuous distribution of seismic sequences and partial stratigraphic loss in some areas. The unconformity surfaces separating seismic sequences exhibit varying structural characteristics in different parts of the basin. Within the depressions, disconformity contacts may be observed, whereas angular unconformity contacts are evident on the slopes of depressions and at the margins of the basin. Seismic profiles demonstrate an uneven distribution of thickness for each sequence, with non-overlapping thickness centers, reflecting variations in the dynamic conditions controlling basin subsidence and sedimentation during different stages of regional tectonic evolution. These observations reveal the fundamental characteristics of the Junggar Basin as a large-scale composite basin.

3. Data and methodology

This study is mainly based on two-dimensional seismic reflection data that constrain basin main faults and several seismic horizons. These seismic sections that are perpendicular to the strike of major faults were used to describe the geometry and architecture of different tectonic units, and display data down to 4–7 s two-way travel time (TWT).

The outcrop data around the Junggar Basin were collected through the field investigation and measurement. Two long field sections were conducted in the study area. Strikes, dips or dip angles of folds and faults were measured to make stereographic projection diagrams and paleo-stress field diagrams in the vicinity of cross-sections.

Based on the interpretation of regional 2-D seismic profiles E-E',

Era	System	Series	Formation	ו	Age, Ma	Thickness, m	Lithology	Basin evolution stage	Tectonic movement
Cenozoic	Quaternary		Xiyu	Q ₁ x	- 2.58 - 23.03 - 33.8 - 38.87 - 65.5 - 72.1 - 85 - 118 - 130 - 145	1200~2470		Foreland compressional basin	Himalayan Movement
	Neogene	Pliocene	Dushanzi	N ₂ d		1300~2000	======		
		Miocene	Taxihe	N₁t		250~330			
			Shawan	N₁s		150~500			
	Paleogene	Oligocene- eocene	Anjihaihe	E ₂₋₃ a		130~780			
		Paleocene	Ziniquanzi	E ₁₋₂ z		150~400			
	Cretaceous	Upper	Honglishan	K₂h		46~813		Uniform sedimentary basin	Yanshan Movement
			Ailikehu	K₂a		22~509			
		Lower	Lianmuqin	K₁/		20~136			
			Shengjinkou	K₁s					
			Hutubihe	K₁h		300~515	\$====		
ا			Qingshuihe	K₁q					
iozo	Jurassic	Upper	Kalazha Qigu	J ₃ k		0~850 580~970		Transpressional flexural basin	
Mesozoic		Middle	Toutunhe	J_3q J_2t	- 163.5 - 168.5 - 174.1 - 190.8 - 199.6 - 235 - 247.2 - 254.14 - 260.4 - 268.8 - 272.3 - 298.9 - 323.2	200~645			
			Xishanyao	J_2x		137~980			
		Lower	Sangonghe	J₁s		150~882			
			Badaowan	J₁b		100~625			
	Triassic	Upper	Baijiantan	T ₃ b		40~300			
		Middle	Karamay	T ₂ k		30~270			Indosinian Movement
		Lower	Baikouquan	T₁b		130~200			
	Permian	Upper	ShangWuerhe	P ₃ w		100~400	3	Compressional basin	Hercynian Movement
		Middle	XiaWuerhe	P ₂ w		100~1450			
			Xiazijie	P ₂ x		850~1160			
zoic		Lower	Fengcheng	P₁f		430~1700	2////		
Paleozoic			Jiamuhe	P₁ <i>j</i>		400~1800	2		
	Carboniferous .	Upper		C ₂			/x x(Extensional faulted basin	
		Lower		C ₁			(
X)		77	Conglomerate		Sandston	ле <u> </u>	=		Mudstone Unconformity

Fig. 2. Generalized litho-stratigraphic chart of the Junggar Basin and its adjacent regions from Carboniferous to Quaternary, showing 5 main tectonic evolution stages (modified from He et al., 2018).

a NW-SE trend balanced cross-sections in the middle of the basin were made utilizing ^{2D}Move software, and mostly maintained area balancing during restoration procedures. The location of cross-section can be found in Fig. 1, oriented perpendicular to the main structural trend. Notably, in the Junggar Basin, significant lateral variations exist in lithology, thickness, and burial depth across various tectonic units. These variations may lead to lateral differences in compaction, consequently complicating the process of decompaction. Hence, decompaction was not accounted for during balanced-section restoration during this study.

The stratigraphic unconformity is indicative of regional tectonic events and serve as markers for delineating stages of regional tectonic evolution. In sedimentary basins, there are also regional unconformities, which serve as important criteria for dividing the stages of basin tectonic evolution. In this study, additionally,

variations in the rates of basin subsidence and sedimentation between different stages may exist. Utilizing the principles of stratigraphic stripping, sedimentation curves can also reflect the stagewise development of a basin.

In this study, based on the field observations and measurements of different types of faults, conjugate shear joints and fault slickensides in different parts of the basin. The Stereographic projection method and Stereonet software were applied to restore the direction of the paleotectonic stress of the study area, and the characteristics and evolutionary law of the paleo-stress field were analyzed.

Analogue modelling has been widely applied in the study of geological deformation and evolution of basins (Yan et al., 2016), orogenic belts (Rahe et al., 1998; Bonini et al., 1999; Rossetti et al., 2000), and plate collision scales (Davy and Cobbold, 1991;

Persson and Sokoutis, 2002; Moore et al., 2005). During the experimental process, the use of digital camera can record the deformation process of the model in detail and provide good visualization results. in addition, the boundary conditions of physical simulation experiments are easy to set and change. The model proposed here has been geometrically, kinematically, and dynamically scaled to the Junggar Basin. Geometric similarity is achieved with a thickness ratio of approximately 1.0×10^{-5} , where 1 cm of dry loose quartz sand in the model represents 1 km of sediment in the natural setting. The dry quartz sand, with an average internal friction angle ranging from 31° to 33° and cohesive strength of 1.05 kPa, is employed as an appropriate material for simulating brittle deformation of upper crustal sediment according to the principles of Mohr-Coulomb failure (McClay and Buchanan, 1992). The quartz sand particles exhibit a rounded shape, with a grain size of approximately 0.2 mm.

By simulating the physical properties of sedimentary units in the Junggar Basin with appropriate modeling materials, a comparable dynamic has been achieved. In this regard, it is essential to incorporate intrinsic material characteristics such as cohesion (τ_0) and internal friction coefficient (μ) into the approximate models and properties (Koyi and Kenneth, 1993; Koyi, 1997). The average internal friction angle for rocks in the upper crust (<10 km) is approximately 40° (Brace and Kohlstedt, 1980), yielding an internal friction coefficient (μ) of 0.84. The internal friction angle for the unconsolidated loose sand used in the model is 31°–33°, resulting in an internal friction coefficient of 0.73 (Koyi and Vendeville, 2003; Yu and Koyi, 2016, 2017), which is reasonably close to the internal friction coefficient of upper crustal rocks. Simultaneously, cohesion (τ_0) is scaled through the equality between the dimensionless shear strength in the model and the dimensionless shear strength in the natural setting.

$$\left(\frac{\rho gl}{\tau_0}\right)_{\rm m} = \left(\frac{\rho gl}{\tau_0}\right)_{\rm p} \tag{1}$$

where ρ is density, l is length, g is gravitational acceleration, and subscripts m and n represent model and property, respectively.

The dimensionless ratio between the model and the natural setting is calculated by employing shear strength values for sedimentary rocks in the range of 1–10 MPa. For clastic sediments, shear strength and density are taken as 10 MPa and 2550 kg/m³, respectively. The cohesion of dry loose sand is about 100–140 Pa, with a density of 1550 kg/m³ (Yu and Koyi, 2016). These properties result in a dimensionless shear strength for the model (Eq. (1)) ranging from 11 to 15, while the natural setting yields a value of 25 (Yu et al., 2021). The proximity of these two ratios within the same order of magnitude indicates the approximate dynamic similarity between our model and the prototype.

According to the scaling process, the scaling stress (σ^*) is given by the following equation (Weijermars and Schmeling, 1986). Consequently, the computed σ^* is approximately 0.54 \times 10⁻⁶:

$$\sigma^* = \frac{\sigma_{\rm m}}{\sigma_{\rm n}} = \rho^* g^* l^* = \frac{\rho_{\rm m} g_{\rm m} l_{\rm m}}{\rho_{\rm n} g_{\rm n} l_{\rm n}} \tag{2}$$

where the subscript m stands for model, and n stands for nature.

4. Multi-phase superimposed deformation characteristics

4.1. Criteria for tectonic evolutionary division

Seismic profile interpretations and field observation reveal the presence of four regional first-order unconformities in the entire Junggar Basin, including the bottom layer of the Permian, Triassic, Cretaceous, and Neogene. Additionally, the Jurassic bottom, the Paleogene bottom and upper-middle Permian bottom also constitute unconformities, primarily distributed along the margins of the basin or uplifts.

The EW-oriented seismic profile (Fig. 3(a), (b)) crossing the eastern slope belt of the Junggar Basin illustrates regional angular unconformity contacts between the Paleogene, Cretaceous, Triassic, Permian strata, and their underlying formations. Similar unconformity structures revealed by this seismic profile are observable in other regions within the basin. Notably, the unconformity between the Cretaceous and underlying formations is particularly distinct, and folding deformation of the Jurassic strata with erosion and subsequent coverage by the Cretaceous, is evident at various locations within the basin (Fig. 3(c), (d)).

Moreover, prominent angular unconformities are observable at the outcrop observation along the west margin (Fig. 4(a), (b)) and southern margin (Fig. 4(c)) of the basin. The attitudes of the strata indicate that there are certain angular differences between the Cretaceous and underlaying Jurassic folds, the Paleogene and underlaying Cretaceous, as well as the Neogene and the underlaying Paleogene. After the underlying strata undergo folding deformation, the new strata draped over the anticlines also undergo folding during later deformation. These phenomena reveal the inheritance and periodicity of thrust folding in the Jurassic and overlying strata, are also important indicators of the phased evolution of basin structures.

Theoretically, the ratio of subsidence rates at different observation points within the same basin remains constant during the same tectonic evolution stage. In this study, by comparing the burial depth variations between different locations, we can approximately delineate the multi-phase evolution of the basin. Fig. 5 illustrates the contrast in burial depths on seismic profiles between two observation points (A, B) on the slope of the south part of the Junggar Basin and a reference point (P) located in the central part of the Fukang Depression. Since there are no large-scale regional fault structures between these observation points, variations in the slope of the curves indicate changes in basin basement subsidence, reflecting variations in the ratio of subsidence rates in different regions on the same block. The inflection points on the curves reflect the presence of regional unconformities. Similarly, the subsidence of the same observation point at different times can also reflect the staged evolution of the basin. These data collectively indicate the presence of regional unconformities at the base boundaries of the Neogene, Cretaceous, Jurassic, and Triassic in the basin. Using these unconformity surfaces as markers, significant changes in the tectonic nature of the basin have been made.

The vertical coordinate represents the burial depth of each layer interface at the reference point P identified on the seismic profile, the horizontal coordinate represents the difference between the burial depth of the layer identified on the seismic profile by the observation points and the reference point.

4.2. Division of tectonic phases

Based on the internal unconformity characteristics within the basin, combined with regional tectonic events and deformation analysis, we divided the tectonic evolution of the Junggar Basin into five phases: Late Carboniferous—Early Permian (D₁), Middle—Late Permian (D₂), Triassic—Jurassic (D₃), Cretaceous—Paleogene (D₄), and Neogene—Quaternary (D₅) (Fig. 6). The Carboniferous—Early Permian phase represented the final consolidation phase of the peripheral continental margin basin surrounding the Junggar ancient landmass, forming the basement of the Junggar Basin. Subsequently, the following four phases are controlled by different tectonic dynamic factors, led to the formation of four different

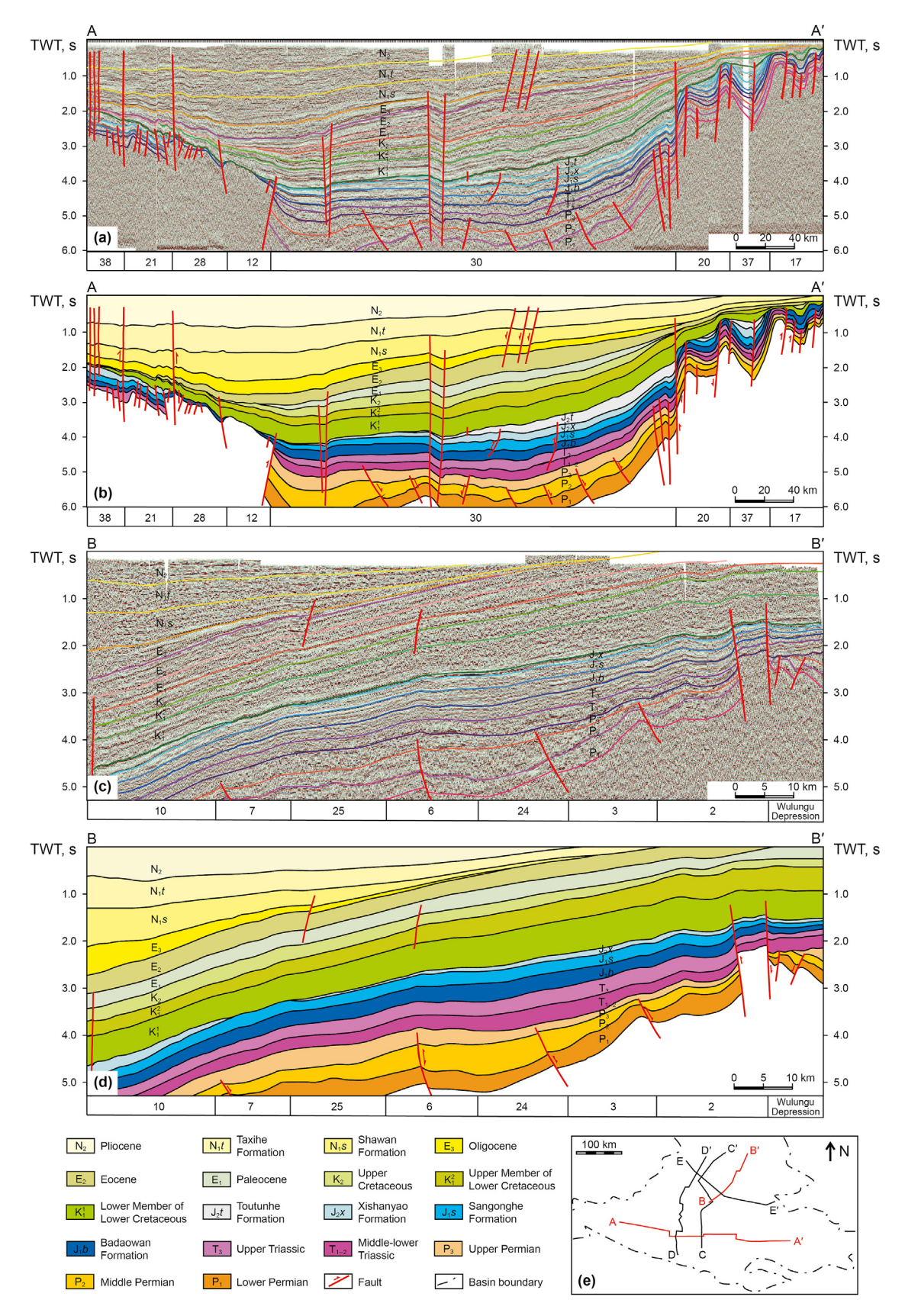


Fig. 3. Seismic sections through the Junggar Basin showing the main regional unconformities and their deformations of different parts, the numbers below the figure represent different tectonic units, see specific location in Fig. 1. Explained W-E trending seismic section A-A' showing the unconformity contact between Cretaceous and underlaying strata, Upper Permian and Lower Triassic (a); geological interpretation of seismic section A-A' showing the main structural styles of middle Junggar Basin (b); explained NE-SW trending seismic section B-B' in the north part of the basin showing the unconformity contact between Upper Permian and Lower Triassic (c); geological interpretation of seismic section B-B' showing the main structural styles of northeast Junggar Basin (d); seismic section locations are given in (e).

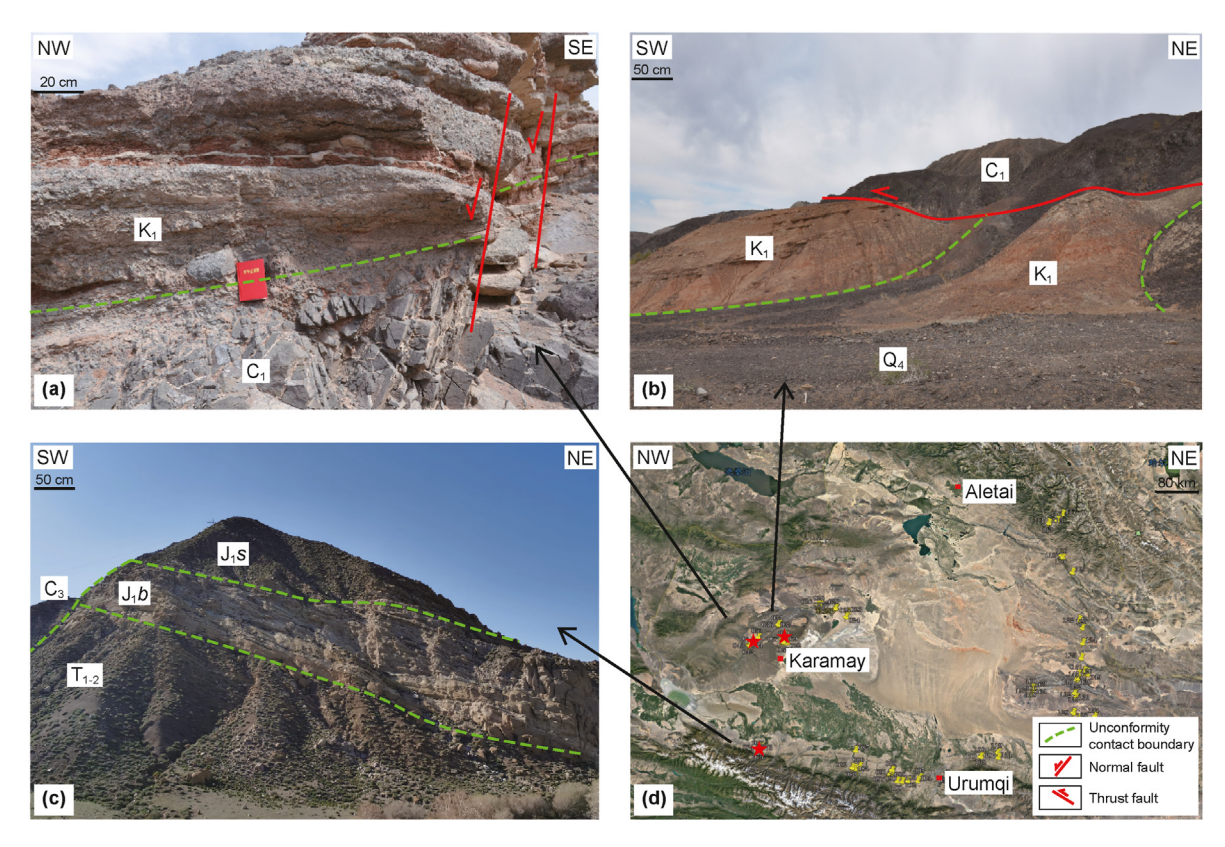


Fig. 4. Field photographs of unconformity contact in west and south margin of the Junggar Basin. Overlapping unconformity between upper Cretaceous and upper Carboniferous in western part of the basin (a, b); angular unconformity between Badaowan Formation and Triassic, disconformity between Badaowan Formation and Sangonghe Formation in south margin of the basin (c); see outcrop location in (d), basemap from Google Earth.

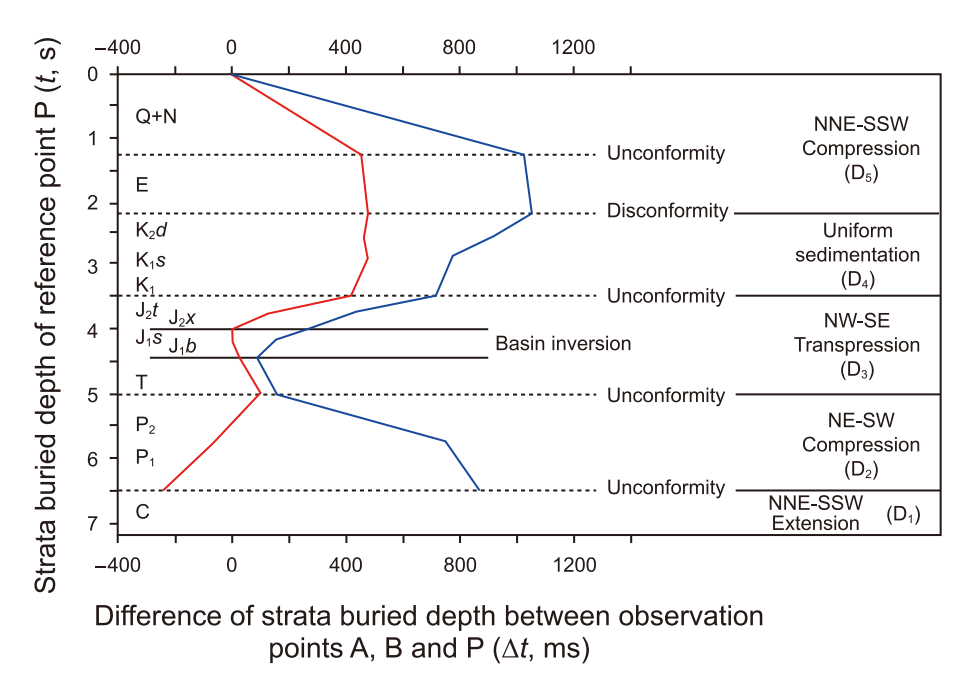


Fig. 5. Comparison of buried depth curves of three points in southern Junggar Basin.

types of sedimentary basins.

(1) First deformation (D_1): NNE-SSW extension

Due to the multiplicity of seismic interpretation, there are still

differing opinions among scholars regarding the nature of the Early Permian basin in the Junggar Basin. Lai et al. (1999), Chen et al. (2001) defined the Late Carboniferous—Early Permian as a foreland basin based on characteristics of terrigenous detrital sediments and stratigraphic sequence features. However, Fang et al.

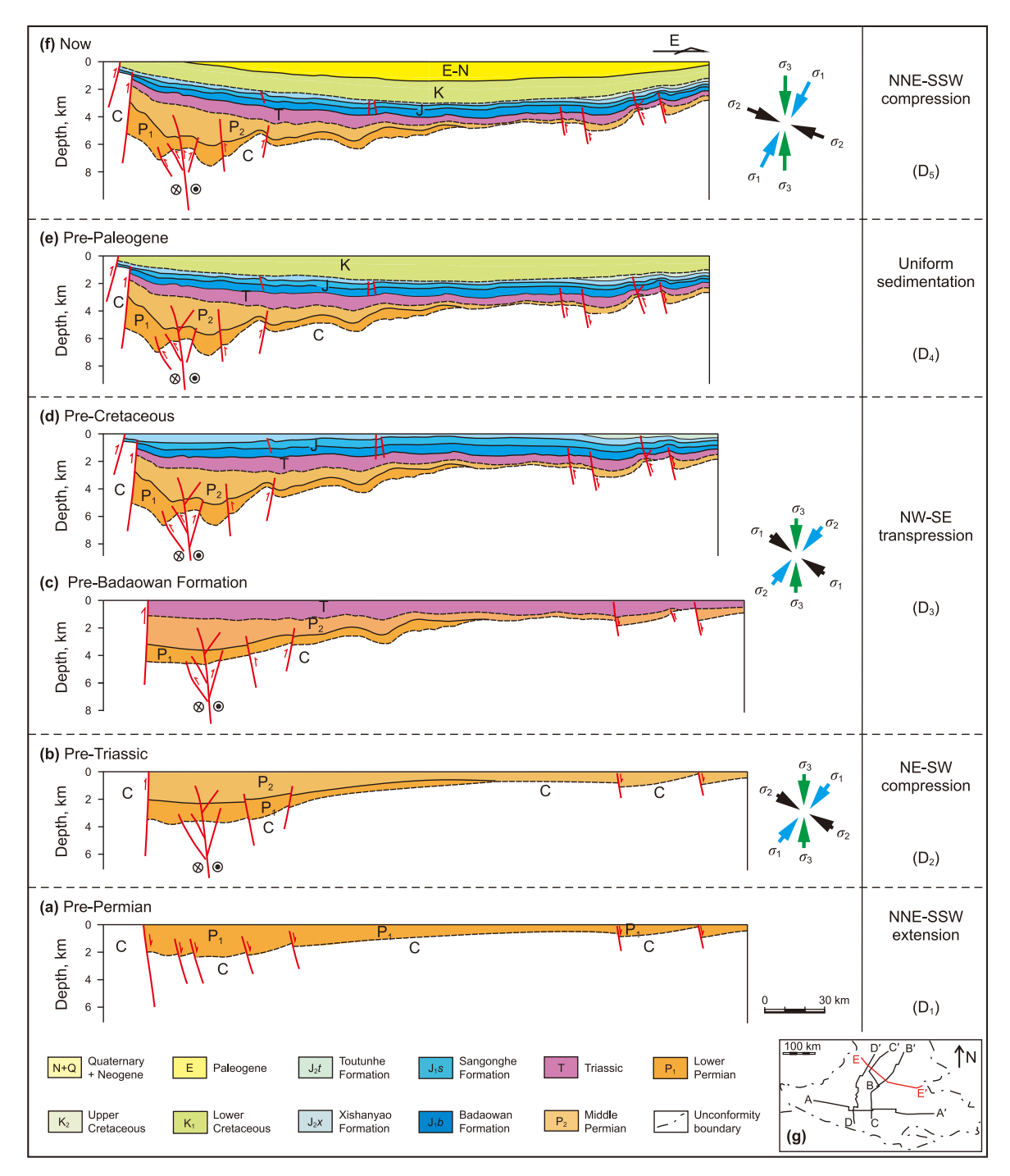


Fig. 6. NW-EW trending tectonic balanced evolution profile E-E' of the Junggar Basin. Structural style before the Permian deposition (a); structural style before the Triassic deposition and stress direction diagram (b); structural style before Badaowan Formation, Cretaceous System (c); structural style before Cretaceous and stress direction diagram (d); structural style before Paleogene (e); present structural style (f); seismic profile (E-E') location is given in (g).

(2006), Rao et al. (2018), and He et al. (2018) considered this period to belong to a rift basin based on systematic comparison of drilling profiles and basin thermal history restoration methods. In this study, we favor defining the basin during this period as an extensional rift basin. In terms of tectonic dynamics, compression can cause the deformation of weak zones around hard land blocks to become stronger and become linear structural zones. However, it is difficult to cause the hard land blocks to rupture themselves. Even if rupture occurs, it is mainly in the form of conjugate translational fault zones, and generally does not produce thrust faults involving

the basement. The hinterland of the Junggar Basin is basically located on the pre-Sinian crystalline basement, and the faults controlling the Middle and Late Permian basins have real distribution characteristics. Its original occurrence is more reasonable to interpret with normal faults.

During this period, the small-scale opening and closing of the northern and southern continental margins of the Junggar-Tuha paleolatitude block was characterized by active continental margins. The northeast land margin of the Junggar paleolatitude block comprised island arcs and inter-arc basins, post-arc basins, and

residual ocean basins. The western land margin of the Junggar paleolatitude block comprised island arcs and post-arc basins as well as residual ocean basins. The southern land margin of the Junggar paleolatitude block initially presented as a passive continental margin and then later became a residual ocean basin. Regional rifting occurred in the Early Carboniferous, and the ocean basins converged in the Middle and Late Carboniferous. In the Bogda Mountains and other places, inherited rifting occurred after the orogenic period, characterized by NE-oriented faulting in the eastern part of the southern margin and NE-NNE-oriented faulting in the western margin, dominated by normal faulting activities. Multi-directional normal faults or strike-slip positive flower structures were present in the basin, and small graben and halfgraben fault trap structures were present (Fig. 3(a) and Fig. 7); some faults exhibited positive and reverse structures due to late compression.

(2) Second deformation (D₂): NE-SW compression

The nature of stresses in the Middle and Late Permian basins changed to mainly NE-SW-oriented compressional stress. The faults controlling the Middle and Upper Permian at the basin margins were mostly steeply dipping reverse faults, while in the interior of the basin, they were steeply dipping normal faults or nearly upright faults. For example, steeply dipping orthotropic

faults were observed in the D-D' and C-C' seismic profiles, and the Middle and Upper Permian faults were distributed on the upper plate (Fig. 7). In the joint north-south basin lineage, the remaining Middle and Upper Permian was cut by the steeply dipping faults, yielding a graben-basin interval. Some faults that cut only to the Permian were observed in the seismic section. Some basement faults that cut upward to the Triassic and Jurassic because of the obvious difference between the Permian of the two plates were considered as having obvious activity during the development of the Permian basin, and some of these faults may have experienced Hesperian faulting around the Junggar paleosol. The Middle and Late Permian basin prototypes were severely modified by late tectonic action, especially by the basin margin fault zones. At this time, the Kelameili tectonic zone in the eastern part of the basin is subjected to NE-SW compressional stress, with faults predominantly oriented nearly perpendicular to the stress direction. Consequently, this fault zone has primarily undergone thrust faulting, resulting in thrust deformation propagating from northeast to southwest. Short distance thrust nappe structures occurred in the eastern part of Dishuiquan (Fig. 8). The Silurian shale thrusts overlied the Carboniferous purple mudstone and limestone, forming structural units such as klippes and tectonic windows. Scratch marks on the fault plane indicate thrusting towards the southeast (200°). Additionally, nearly horizontal scratch marks are visible on the exposed Carboniferous rock layers at the leading edge of the

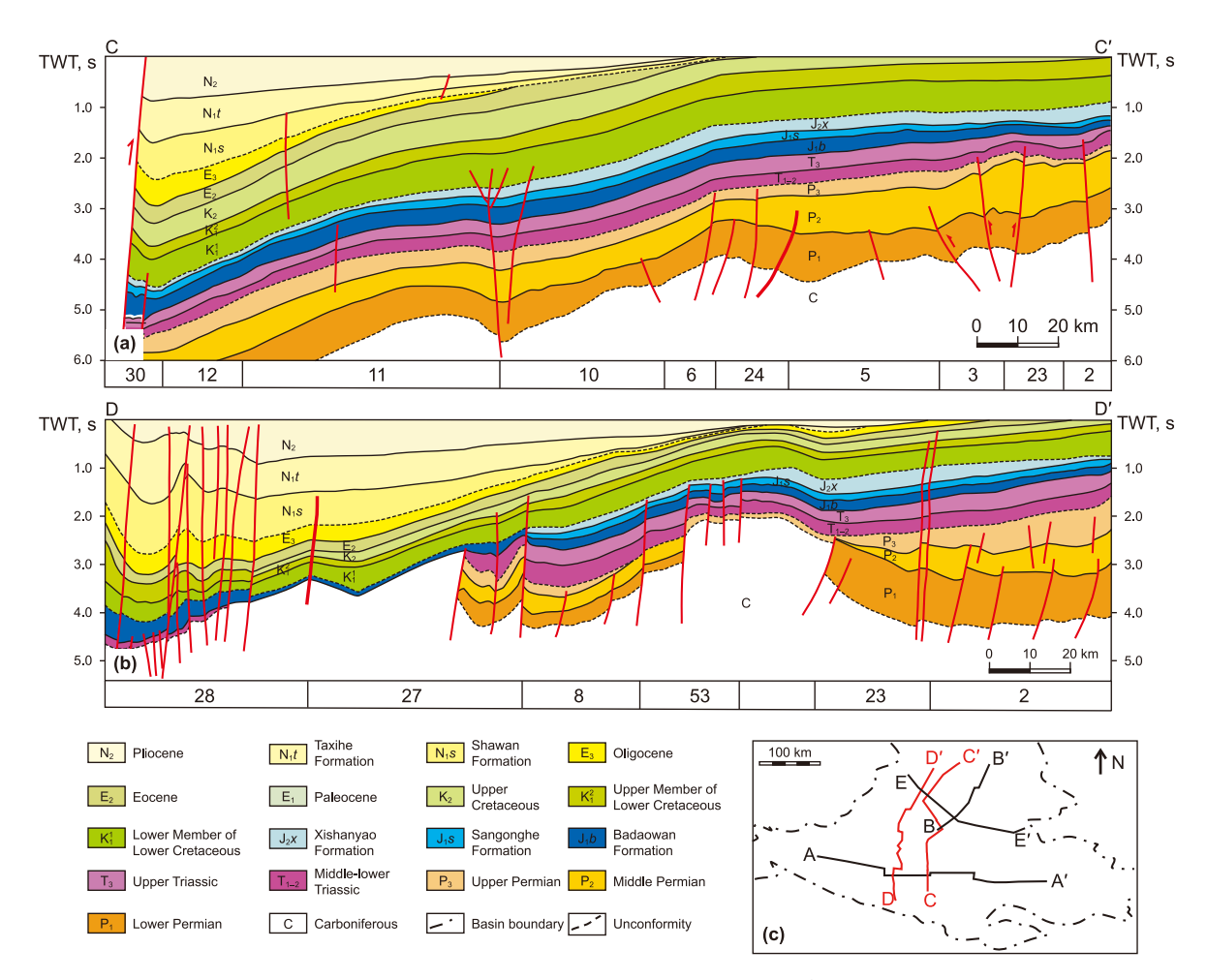


Fig. 7. Geological interpretation of near S–N trending sections. Geological interpretation of seismic section C–C' showing flower structures and strike-slip faults formed by transpressional stress in the middle part of the basin (a); geological interpretation of seismic section D-D' showing the structural styles of midwest part of Junggar Basin, the Permian-Triassic pinched out in the southern margin (b); seismic section locations are given in (c).

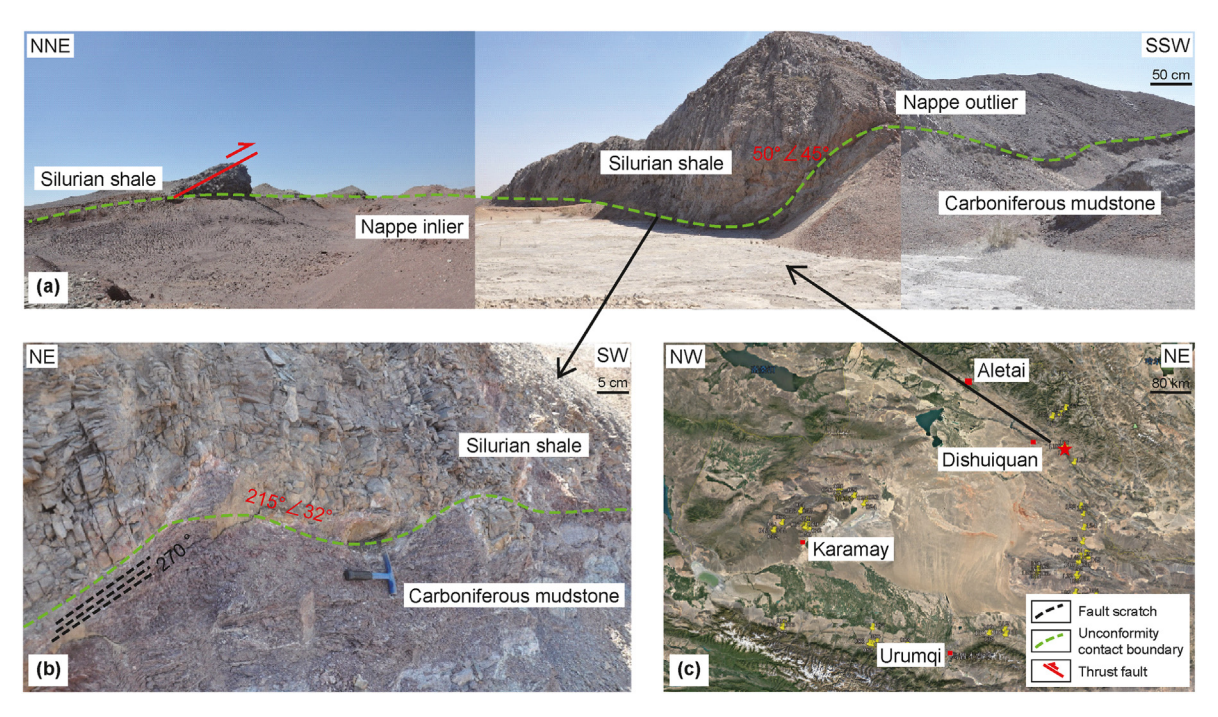


Fig. 8. Deformation of compression thrust structure during Middle-Late Permian. Thrust nappe structure can be seen in the eastern part of the Junggar Basin, Silurian shale covering the Carboniferous mudstone as nappe outlier (a); unconformity contact between Silurian and Carboniferous (b); see outcrop location in (c), basemap from Google Earth.

thrust sheet, indicating thrusting towards the southeast (200°) based on the tilt direction of the steps. The steeply dipping reverse faults controlling the distribution of the Middle and Upper Permian seen in the seismic section may have stemmed from the yield changes of the early normal faults during the later structural deformation. The transpressional thrust faults controlling the boundary of the Permian basin were present at the northwest margin of the basin.

(3) Third deformation (D₃): NW-SE transpression

The Indosinian and Yanshan Movement (mainly the latter) generated nearly NNW-SSE trending compressional stress, forming NNE trending transpressional flower structures (Fig. 7(a)) and folds. The structural deformation of this phase and the associated Triassic-Jurassic sedimentation was superimposed on the Permian NW-trending uplift and depression pattern. Simultaneously, it induced the sinistral strike-slip displacement of the NWWtrending basement faults, resulting in regional transpressional deformation within the basin and controlling its subsidence. Under the action of nearly E-W compressive stress, the fault scratches, and steps of sinistral movement, with an average strike of 270° can be seen on the fault planes (Fig. 8(b)) within the main fault zone in the Kelameili structure zone, east part of Junggar Basin. A strike slip fault can be seen on the seismic profile near the fault zone, indicating that the strike slip structural zone extends towards the interior of the basin and may be connected to the Luliang Uplift Zone, causing it to move northwestward. The tectonic movement in this phase was induced by the closure of Tethys from the east to west, the folded uplift of the Bangong-Nujiang belt, and the remote effect of the formation of the Tsetse-Nagu Yanshan orogenic belt leading to the reactivity of the intraplate basement fractures. Consequently, the NEE-trending uplift belt, depressional belt, and several groups of faults of different nature developed in the basin.

(4) Forth deformation (D₄): Uniform sedimentation

After the deposition of the Middle and Late Jurassic, the basin entered the phase of denudation and peneplanation. The basin deformation was weak in Cretaceous-Paleocene, and the different types of folding and fracturing were not obvious. During this phase, vertical loading (primarily from sedimentary deposits) caused crustal deformation, leading to surface subsidence. This was manifested as balanced basement subsidence with relatively stable stratigraphic thickness and petrography. The Early Cretaceous basin was the widely distributed, overlying the bedrock at the edge of the basin, with the greatest subsidence, forming a uniform depression. Its sedimentary center migrated southward to the middle of the basin. The Late Cretaceous prototype basin started shrinking, the distribution range decreased, the deposition and subsidence amplitude weakened, and the overall tectonic pattern exhibited a northern slope and southern depression. Three depositional centers developed, among which a low amplitude uplift developed between the Changji Depression and Shawan Depression.

(5) Fifth deformation (D₅): NNE-SSW compression

Since the Neogene, with the strong subduction of the Asian-European plate and the rapid uplift of the North Tianshan Mountains, three rows of imbricate-like retrograde fold zones gradually developed on the southern margin of the basin, and abundant tear faults and thrust faults developed in the northern part of the mountain (Fig. 9(a), (b)), due to the basal coal layers and the difference in the movement rate between the plates (Shen et al., 2022). In the northern part of the basin, frontal uplift developed in the Luliang and Wulungu areas, with sediments rapidly overlying and thinning from the foreland to the frontal uplift, creating a typical wedge-shaped basin geometry. Under the control of the N-S compressional stress, numerous nearly N-S trending normal faults developed along the western margin of the basin. Additionally, on top of the NE-trending fold structures formed during the Lower Jurassic, Neogene unconformities developed in the eastern Junggar area.

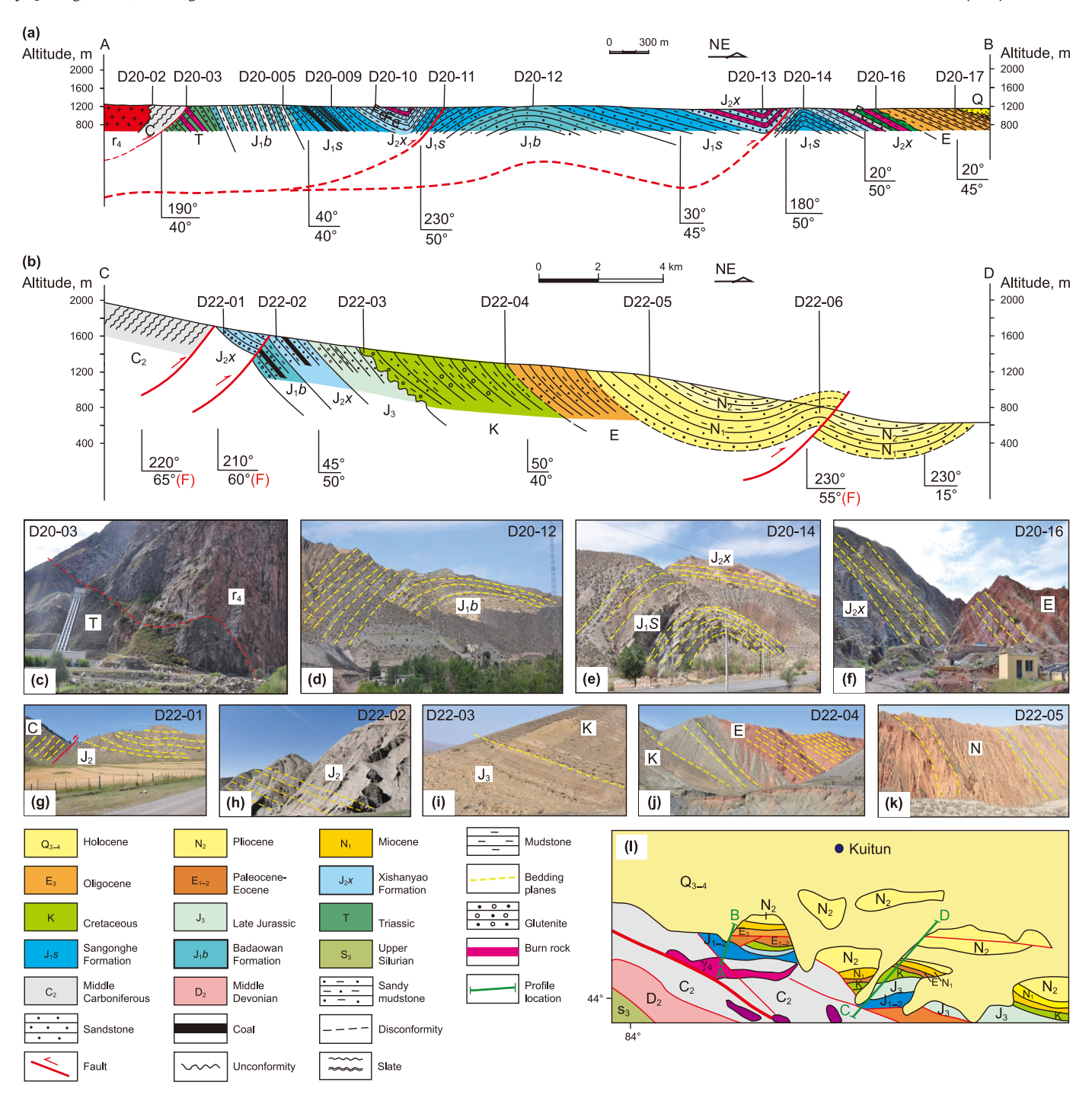


Fig. 9. Field photographs and Cross-section maps of the D_4 deformation and D_5 deformation. Geological cross-section map of Sikeshu Area (a); geological cross-section map of Anjihai Area (b); intrusive contact phenomenon in Carboniferous strata (c); folds in Xishanyao Formation and Badaowan Formation in southern margin of the Junggar Basin (d, e); unconformity contact between Xishanyao Formation, Jurassic System and Eogene (f); thrust fault during D_5 deformation (g); disconformity between upper Jurassic and Cretaceous (h, i); unconformity between Cretaceous and Eogene (j); Neogene folds formed syncline (k); the photo number corresponds to the position number on the section. See cross-section location in geological map of the southern margin of the Junggar Basin (l).

The five phases of the non-coaxial stress field have resulted in the formation of the current tectonic framework of the Junggar Basin, and the formation and evolution of the basin exhibit obvious stages. However, comprehensively reflecting the mechanical factors affecting the deformation for the evolution of the large, superimposed structures at the basin-mountain scale using only the restoration of balanced sections is difficult. The quantitative description of the superimposed structures can be improved

through the description and statistics of the occurrence of field fractures, joints, and scratches, which plays an important role in the study of their genetic mechanisms.

4.3. Paleo-stress field characteristics

During the fieldwork, a statistical analysis of the folded structures, fault planes, scratches, and joints in the outcrop area of the

Junggar Basin was conducted, and a diagram of the main faults and stress field distribution direction in the study was made (Fig. 10). The basic principle of polar stereographic projection is to project a construction surface (or line) through the center of the projection sphere, with the upper pole of the sphere as the emission point, and project the intersection of the structure surface (or line) and the lower hemisphere sphere onto the equatorial plane to obtain the relationship between its orientation and angular distance. The results show that the stress field directions of the different places of the basin were not completely the same during certain tectonic evolution phase, and the main characteristics of the paleo-stress field in different periods were as follows.

- (1) The Cenozoic faults and joints were along the NNE direction of the stress field, which is equivalent to D_5 deformation phase mentioned above, and the paleo-stress directions were basically the same in the southern, eastern, and western margins (stereographic projections and joint rose diagrams marked with 3 in Fig. 10).
- (2) The characteristics of the Mesozoic stress-field are relatively complex (stereographic projections marked with ② in Fig. 10), representing D₃ deformation phase during the evolution of the Junggar Basin. The stress field direction of the Triassic to Jurassic is NNW-SSE, which is consistent in the northwest and south margins of the basin. In the east part of the basin, the statistical results of the fault planes and scratches in the Kelameili Suture Zone showed a nearly E-W trend, while the Fuyun Strike-slip Zone in the north of it showed an NNW-SSE trend stress field, which is similar to the results of northwest margin of the basin. The formation of anomalous stress fields in different basin areas may be closely associated with the deformation of distinct tectonic

- zones and interactions along plate margins. Simultaneously, it may also be related to the distribution patterns of pre-existing faults in the basement.
- (3) The statistical results of the Middle and Late Permian were different (stereographic projections marked with ⊕ in Fig. 10). The folds and joints in the northwest margin exhibiting NW-SE orientation, while those in the east exhibiting NNE-SSW compression, reflecting the sources of stress in different directions. This result indicates that the northwestern margin of the basin was more influenced by the Kazakhstan plate during the Middle and Late Permian.

4.4. Three-dimensional basin tectonic evolution model

By statistically analyzing the evolutionary characteristics of paleo-stress fields in different phases and clarified the tectonic evolution history of study area with the evidence mentioned above, a three-dimensional model of the tectonic evolution of the Junggar Basin was established herein (Fig. 11).

(1) D₁ —Carboniferous to Early Permian extensional deformation

In the Early Permian, a series of subparallel central fault zones, the Wulungu fault zone, the Luliang uplift zone, and the North Tianshan uplift zone formed under the NNE-SSW extensional stress. During this phase, the Dalbout Fault in the northwest margin of the basin experienced dextral transtensional activity and Lower Permian massive conglomerates were deposited. The Kelameili tectonic zone in the northeast margin underwent dextral shear deformation and formed a tough-brittle shear zone with S

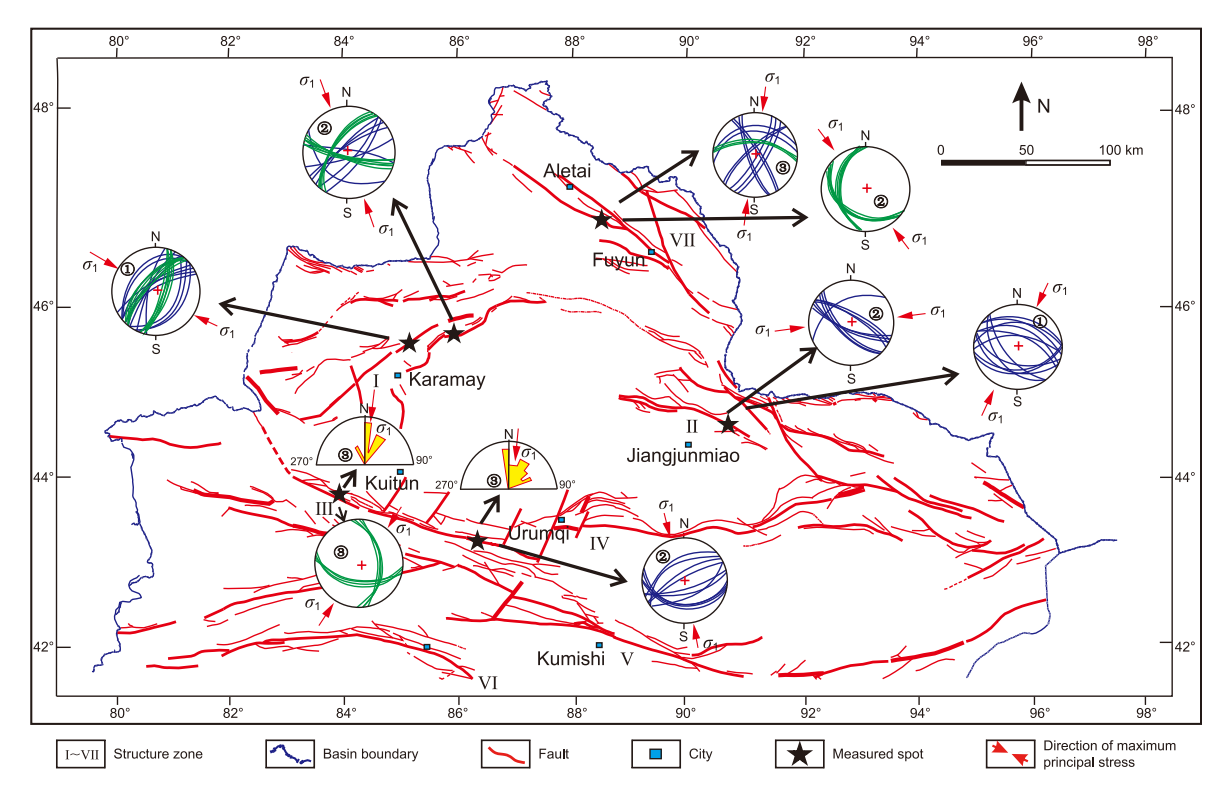


Fig. 10. Paleo-stress field diagram of the Junggar Basin. I—Dalbot Suture zone (Strike-slip zone); II—Kelameili Suture zone (Strike-slip zone); III—Yishan Suture zone; IV—Bogda Mountain Suture zone; V—Kumishi Suture zone; VI—Songshudaban Suture zone; VII—Fuyun Strike-slip zone. (①—Compressive stress field during Middle-Late Permian; ②—compressive stress field during Triassic to Jurassic; ③—compressive stress field during Cenozoic; blue projection lines modified from Song et al., 2015; green projection lines are measured in this study).

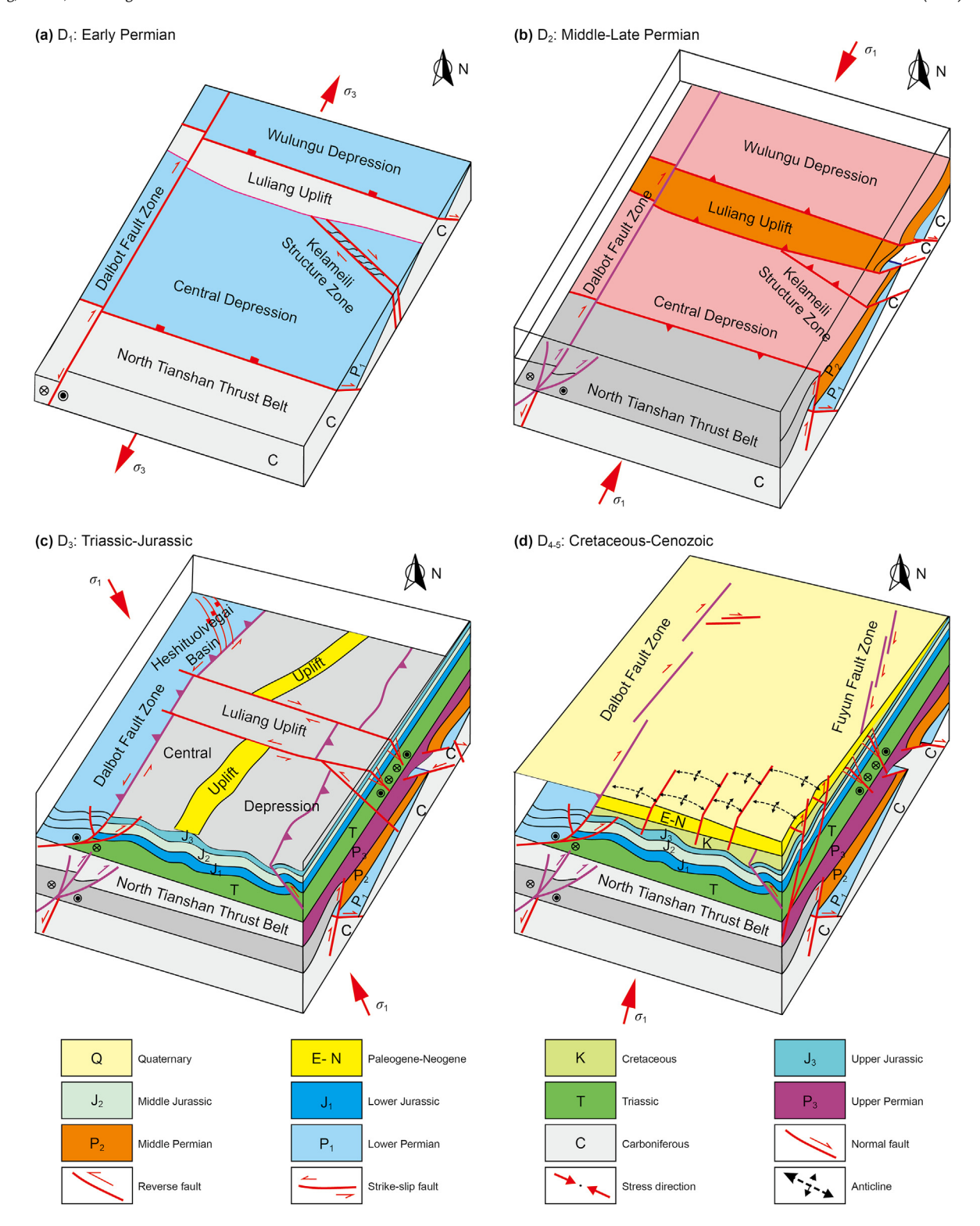


Fig. 11. Three-dimensional tectonic evolution model of the Junggar Basin. Tectonic units during early Permian and the orientation of principal stress (a), forming the basement fault system of the basin; tectonic units during Middle to Late Permian and the orientation of principal stress (b), more reverse faults formed at this time; tectonic units during Triassic to Jurassic and the orientation of principal stress (c), a large number of folds and faults formed; tectonic units and structural style during Cretaceous to Cenozoic, and the orientation of principal stress (d), three rows of tear faults formed in the southern margin of the basin and gradually formed the present tectonic pattern.

foliation-C foliation (S-C fabric) (Fig. 11(a)).

(2) D_2 —Middle and Late Permian compressional structural deformation

During the Middle and Late Permian, the rift basin structure formed in the D₁ phase was positively inverted and changed into a paleotectonic pattern of uplifts and depressions (Fig. 11(b)) under the NE-SW compressional stress. In the central part of the basin, the uplift zone of land-beam was affected by extrusion and uplift, resulting in the thinning or removal of the Lower Permian. In the southern margin, large overthrust structures formed to the north. In the northwest margin, the Karamay-Baikouquan and Urho-Xiazijie overthrust tectonic zones formed, and the fault zone comprised a series of arc-shaped reverse faults, reverse mask faults, and the interposed fault blocks. A large number of faults were backplunging faults in the direction of the basin, and they exhibited right-sided slip activity. In the southwest margin, the Hongshanzui-Chepaizi fault zone developed, comprising an arc-shaped spreading along the direction of the mountain system in plane view, and a listric imbricate fan combination developed in these cross-sections, which belonged to the basement-involved thrust style. Along the south margin, a series of high-angle back-plunging structures developed.

In this phase, part of the basin belonged to the torsional subsidence, or the weak compressional subsidence basin controlled by the strike-slip faults, but we believe that the soft linkage between the ancient land masses or ancient island arcs in this period did not cause high uplifts and that no millstone construction occurred. Therefore, it cannot be classified as the foreland basin stage.

(3) D₃ —Triassic-Jurassic transpressional structural deformation

The NNW-SSE trending compression generated by the Yanshan movement caused the northwest and northeast margins of the basin to extrude and thrust toward the basin, forming a superimposed tectonic pattern of NNE-trending backward thrusts. This resulted in oblique interactions on the basis of D₂ (Fig. 11(c)), with the Chepaizi-Mosowan paleo-lift as a typical representative. Simultaneously, it induced leftward displacement of the NWtrending basement faults, which caused transpressional deformation in the basin area. During this phase, leftward compressional stress occurred in the pre-existing deep faults on the western margin of the basin, and rightward slip activities occurred in the Kelameili fault on the eastern margin. The slip activities of the two major marginal faults led to the formation of secondary slipassociated structures in the basin. In the western margin of the basin, the transpressional stress of the Dalbout fault intensified and controlled the deposition of the Jurassic in the Heshituolvegai Basin. The significant uplift of the eastern side of the fault led to the loss of Jurassic strata in that region.

(4) D_{4-5} —Paleocene to Quaternary foreland thrust structural deformation

Influenced by the remote effect of the subduction collision between the Indian plate and the Eurasian continental plate, the North Tianshan Mountains thrusted northward, causing the southern margin of the basin to lift off and form an extrusion-type foreland basin. Subsequently, the Himalayan movement reversed the entire basin to the south and formed multiple rows of slip folding zones with sinistral tear faults in the southern margin (Fig. 11(d)). The punching and compressional stress caused the basement to deflect and sink, forming a frontal zone with a thickness of more than 3000 m of molasse formation. At this time, the

dextral slip faults, with the Fuyun active fault and the Urho asphalt veins as typical representatives, developed at the northern part of the basin.

5. Deformation characteristic analogue modelling

Numerous studies have proven that analogue modelling is effective for studying the tectonic formation processes and genesis mechanisms in petroliferous basins, and it is important for helping geologists understand the evolution of structural deformation at the basin-mountain scale and study the tectonic formation mechanisms (McClay, 1990; Bellahsen et al., 2003). The self-similarity of geological processes and analogue modellings reveal certain similarities between experimental models and natural prototypes, and the similarity of the geometric-kinematic-dynamic processes at different scales forms the theoretical basis of the analogue modelling experiments (Hubbert, 1937; Colletta et al., 1991).

The basis of analogue modelling is deformation geometry, which usually determines the boundary conditions and stress mode of the model according to the deformation patterns of the study object, and only considers the stress direction, not the stress magnitude. Since 1815, when James Hall first used superimposed fabric sheets to simulate the formation of folds in real strata, numerous sandbox experiments have been conducted to verify and restore the evolution of geological structures (Dooley and Schreures, 2012). Reynolds and Holmes (1954) used rubber cement to study the fold superposition patterns. After studying the superposition folds in metamorphic zones and the classification scheme. Ramsay et al. (Ramsay, 1962; Ramsay and Huber, 1987) proposed four different types of superposition fold interference patterns. Numerous simulation results have shown that the structural deformation process is mainly controlled by geometrical conditions and is less related to the rock mechanical properties and stress magnitude (McClay, 1990; Costa and Vendeville, 2002). Therefore, the analogue modelling is the main method used to reproduce the tectonic evolution and to study the behavior of deformation and other problems.

Combining the field geological data and seismic geotectonic analysis of the Junggar Basin, we constructed a model to conduct analogue modelling experiments and perform a comparative study on the tectonic styles of the Junggar Basin. Moreover, combining the analysis of the experimental data and the quantification of the tectonic elements, it is necessary for us to simulate and verify the evolution process and mechanism of the superposition deformation in the study area, and this will provide a theoretical basis for deepening the structural analysis of superimposed basins.

5.1. Experimental materials and model setup

The dimensions of the sandbox experimental setup were 60 cm (L) \times 50 cm (W) \times 30 cm (H), with a fixed rigid metal plate at the bottom. The western boundary of the model was a transparent glass baffle with dimensions of 80 cm (L) \times 20 cm (H) \times 2 cm (thick), and the three sides of the east and south were rigid metal plates connected to the force-applying motor with dimensions of $60 \text{ cm} (L) \times 20 \text{ cm} (H) \times 1.5 \text{ cm} (thick)$, whose deformation effect is negligible. A high-density polyethylene plastic plate with dimensions of 60 cm (L) \times 5 cm (W) \times 2 cm (H) was placed in the middle of the model to simulate the pre-existing paleo-uplift in the middle of Junggar Basin, and the remaining model was paved with gray quartz sand, and the ratio of the sand box model to the actual study area was about 1:100000 (Fig. 12). Dry and loose quartz sand was selected as the experimental material to simulate the real formation as its deformation characteristics are similar to those of brittle formations in the upper crust under the premise that it

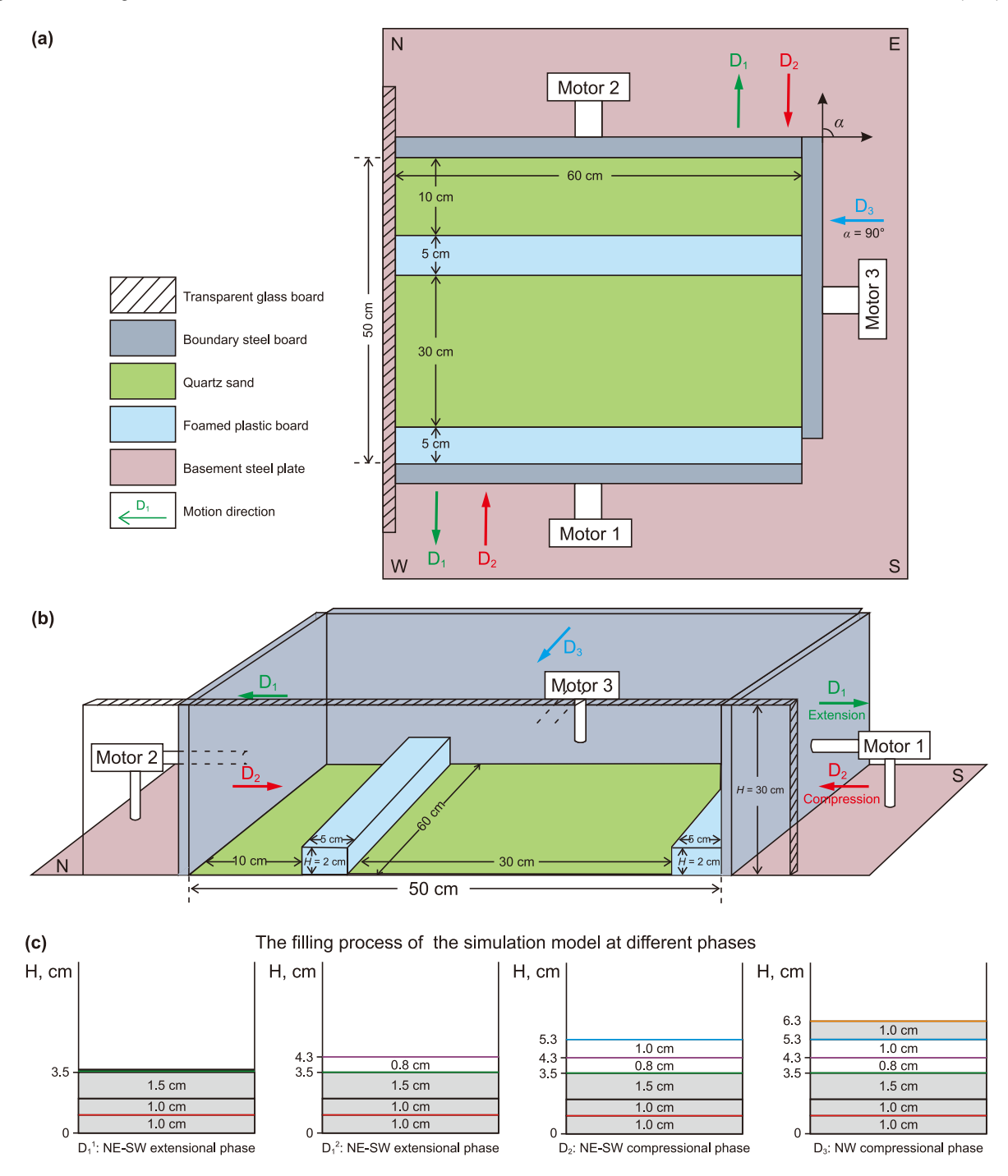


Fig. 12. Schematic of analogue modelling experimental apparatus. Plane of experimental apparatus (a); stereogram of experimental apparatus (b); the filling process of the simulation model at different phases (c); the direction of arrows represents the direction of motion.

Table 1Experimental layer parameters and kinematic feature.

Layer number	Height, cm	Experimental material	Marker color	Kinematic feature	Experimental motion phase	Represent tectonic evolution phase
6	6.3	Gray quartz sand	Red	NW one-side compression 5 cm	D_3	D ₄₋₅
5	5.3	White quartz sand	Blue	NE-SW two-side compression 5 cm	D_2	D_{2-3}
4	4.3	White quartz sand	Pink	NE-SW two-side extension 2 cm	D_1^2	D_1
3	3.5	Gray quartz sand	Green	NE-SW two-side extension 3 cm	D_1^1	D_1
2	2.0	Gray quartz sand	Black	_	_	_
1	1.0	Gray quartz sand	Red	_	-	_

follows the Mohr-Cullen strength criterion. To facilitate the observation and recording of the experimental process, colored quartz sand was used to create the marker layer, and the mechanical properties of the quartz sand after dyeing were kept unchanged. The experimental layer parameters and kinematic features are specified in Table 1.

5.2. Experimental process

① D₁ deformation

The experiments were commenced by laying three layers of gray quartz sand with a total thickness of 3.5 cm, using red, black, and green as marker layer colors, to simulate the pre-Mesozoic boundary of the basement strata. Motor 1 and motor 2 were simultaneously tensioned along both sides of NE-SW with a movement rate of 0.25 cm/min for 12 min and a cumulative tensioning displacement of 3.0 cm.

\bigcirc D₁² deformation

A 0.8-cm thick layer of white quartz sand was laid on top of the deformed sand layer to simulate the J_1 stratum, and pink sand was laid on top of it as a marker layer. Motor 1 and motor 2 were simultaneously tensioned along both sides of NE-SW. The experimental device operated at a tensioning speed of 0.25 cm/min, with a duration of 8 min, and cumulative tensioning displacement was 2.0 cm.

3 D₂ deformation

A 1.0-cm thick layer of white quartz sand was laid on top of the deformed sand layer to simulate the J_2 stratum, with a blue sand layer laid on top of as a marker. Motor 1 and motor 2 were simultaneously compressed along both sides of NE-SW. The compressional speed was 0.25 cm/min, the compressional time was 20 min, and the accumulated compressional displacement was 5.0 cm.

④ D₃ deformation

A 2.0-cm thick layer of gray quartz sand was laid on top of the deformed sand layer to simulate the J_3 stratum, with red sand laid on top of it as a marker layer. Motor 3 was compressed unilaterally along the NW direction. The compressional speed was 0.25 cm/min, with a duration time of 20 min, and the total compressional displacement was 5.0 cm.

After the end of deformation in the last phase, the motor stopped applying force and a 1 cm thick layer of white quartz sand was laid on top of the deformed sand layer. The experimental sand body was moistened with water for 24 h and then sectioned.

5.3. Plane deformation result

① D₁¹ deformation result

In the first extensional phase, when both sides of NE-SW were simultaneously tensioned by 1.5 cm, faults F_1 and F_2 appeared near the baffles at both ends of the model, while multiple normal faults (F_3-F_{10}) appeared in the middle of the model, which combined into multiple groups of graben structural styles with roughly parallel trend. As the extensional displacement was increased to 3.0 cm, the existing faults expanded and developed further, exhibiting obvious fault inheritance, with no new faults observed (Fig. 13(a), (b)).

② D₁² deformation result

In the second extensional phase, when both sides of NE-SW were tensioned to the accumulated displacement of 4.0 cm, the previously developed multiple normal faults appeared, with their development locations were approximately the same as the original fault positions. As the tensioning distance increased to 5.0 cm, the pre-existing faults continued to grow and develop, making the graben combination style more pronounced (Fig. 13(c), (d)).

3 D₂ deformation result

In the early compressional phase, when both sides of NE-SW simultaneously compressed to 2.0 cm and the total contraction amount reached 0.8%, reverse faults F_{21} – F_{24} developed. As the contraction continued and the compressional displacement reached 5.0 cm, the experimental strata were significantly thicked and uplifted, and new reverse faults F_{25} – F_{27} appeared alongside the previously developed faults (Fig. 13(e), (f)).

④ D₃ deformation result

In the last compressional phase, when the direction of the applied force was changed, a more pronounced reverse fault F_{28} developed at the front edge of the model. As the compressional displacement continued increasing to 5.0 cm, the thrust fault F_{28} became more prominent, which verifies the succession of fault activity in the plane. Additionally, a secondary fault F_{29} developed on its southern side (Fig. 13(g), (h)).

5.4. Profile deformation result

5.4.1. NE-SW trending profile

The results of the planar experiments were analyzed by slicing the model in both the NE-SW and NW-SE directions. The NE-SW sections (Fig. 14(a)—(f)), taking section M-N as an example, several reverse faults (f_8 — f_{11}) developed on the left side of the section (south side of the model), and f_1 , f_4 , f_5 on the right side of the section (north side of the model). Among these, reverse fault f_8 and its associated back-thrust fault f_7 together formed an anti-Y-shaped structural style. Furthermore, near the right side of the section (north side of the model), reverse fault f_5 and its back-thrust faults f_6 together formed a pop-up structural style. Normal faults f_{12} and f_{14} developed in the left area of the model, creating a graben structure pattern, while only one normal fault f_3 developed in the middle-right area of the section. This disparity may be attributed to the inheritance of the normal faults formed during the early extensional phase.

5.4.2. NW-SE trending profile

The NW-SE sections (Fig. 14(g)—(1)) showed the development of thrust faults (f_{28} , f_{29} , f_{31} — f_{33}) along the two boundaries of the section, exhibiting the similar combinations of structural styles. Among these, the thrust fault f_{31} and its back-thrust fault f_{33} together formed a pop-up structural style. On the right side of the section (south side of the model), imbricate fan thrust faults (f_{28} and f_{29}) are present. Additionally, the reverse fault f_{29} and its associated back-thrust f_{30} created a pop-up structure as well.

5.4.3. Three-dimensional deformation analysis

The simulation results of the three-dimensional cross-sections show the phenomenon of three phases of non-coaxial compression superimposed on early extension (Fig. 15). The normal faults preserved in the current sections indicate the NE-SW-oriented extensional stress during the D_1 experimental phase, corresponding to the extension of the Carboniferous to Early Permian basin. The bilaterally NE-SW-trending compression in the D_2 phase

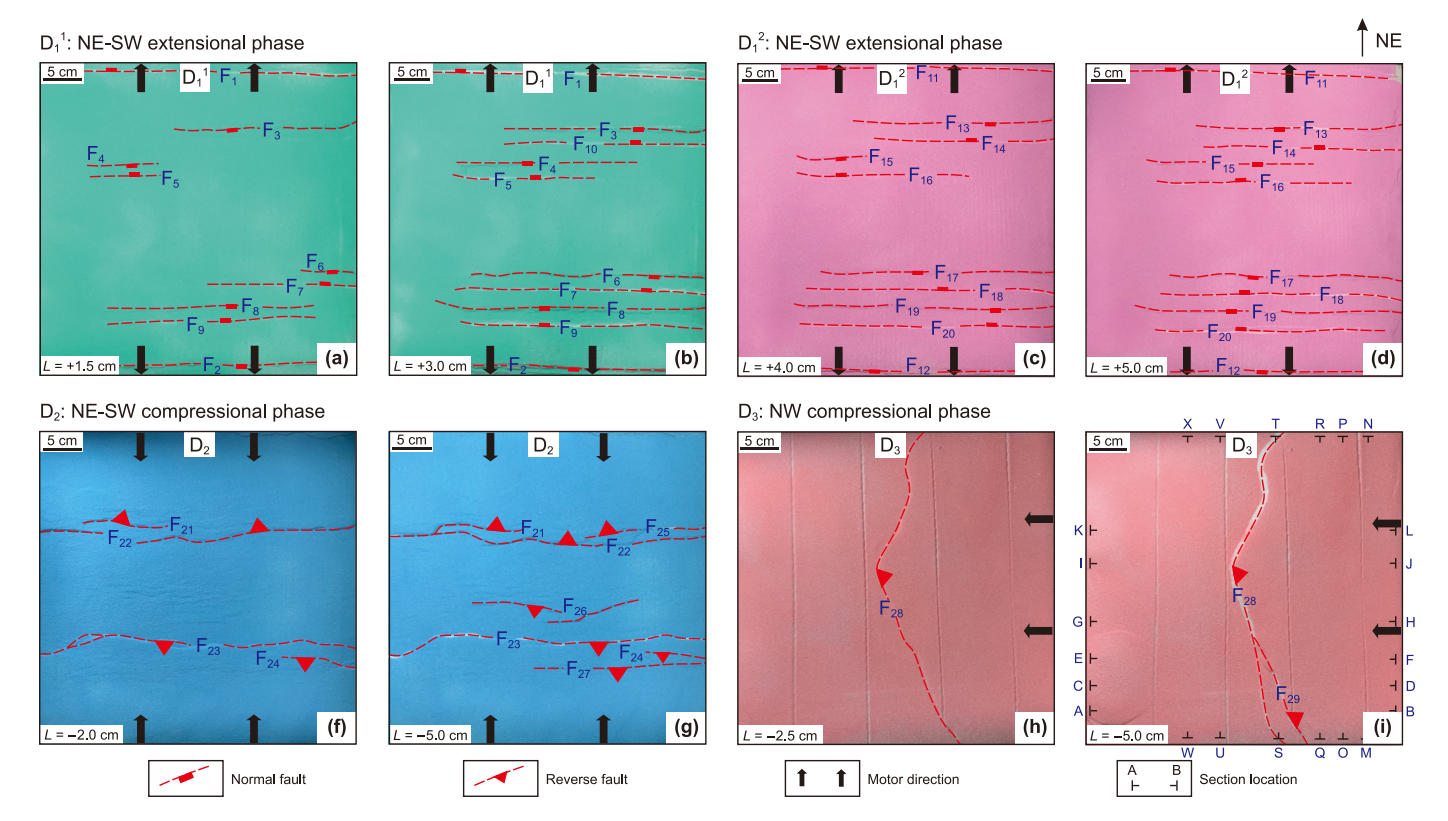


Fig. 13. Experimental top view (photographs and line drawings) of different phases showing the evolution of Junggar Basin from NE-SW extension phase (**a**–**d**) to NE-SW compression phase (**e**, **f**) and SE compression phase (**g**, **h**). "L" represents motion displacement, "+" means elongation, "-" means shortening, arrows represent the direction of motion, the fault label numbers represent the sequence of the faults developed in the experiment.

generated imbricate fan that thrusted toward the basin, along with back-thrust faults in the hanging wall. The simulated results of this phase correspond to the thrust faults formed during the Middle to Late Permian compression phase. During the mid-phase SE-oriented compression, thrust faults and folds structures were formed. The deformations in this phase are equivalent to the NE-trending structural deformation caused by the Triassic-Jurassic compression. In the 3D cross-section model, the lower parts of the faults are seen to overlap with earlier compressional faults, demonstrating the strong inheritance and continuity of the superimposed structures. After the basin has experienced superposition of the anisotropic stress fields, the development location of late-phase faults was closely related to the thickness of the strata. The distance from the nascent faults formation location to the boundary is approximately twice the thickness of the strata, which is consistent with the Anderson's fault theory model. No significant strike-slip deformation was observed during the middle compressional phase, because the slice position was nearly parallel to the compressional direction.

6. Discussion

The results of the analogue modelling experiments revealed that during the late tectonic inversion phase, the compression deformation primarily resulted from the formation of late low-angle thrust faults. Most of the previous normal faults are preserved (e.g., f_{12} , f_{13} , f_{14} , and f_{17} , in Fig. 15(a)–(f)) and only the dip angle is steepened to different degrees. Furthermore, only in the strong thrust tectonic zone, the reverse faults may completely replace the pre-existing normal faults. Consequently, the transformation of all pre-existing normal faults into reverse faults during the later

positive inversion is extremely unlikely, this phenomenon closely linked to the mechanical properties of rocks in the brittle domain: due to the typically steep dip angle of normal faults, the frictional strength along the fault plane during upward sliding is often greater than the rock's fracture strength. This implies that less energy is required to form reverse faults with lower dip angles. Hence, during the process of structural inversion, it is more likely to form new, lower angle thrust faults.

Positive inversion along preexisting normal faults can only be a typically local phenomenon unless certain conditions are met. These conditions include rigid boundary conditions or a small dip angle of the preexisting fault, or the presence of detachment layer on the fault plane. Although Buchanan and McClay (1991), as well as Zhou (1999), used rigid boundary conditions in experiments on rigid basement step faults, rigid boundary listric faults, and rigid boundary half-graben respectively, facilitating inversion along preexisting normal faults during compression phase, the inversion structure is still primarily accomplished through the formation of new low-angle thrust faults. Taking the simulation result as an example, the dip of fault f_1 developed after the late inversion of the preceding normal fault f₃ slowed down (Fig. 15(b)). The experimental results indicate that despite the early occurrence of weak extension and the strong inversion caused by the two phases of compression, the basin boundary still retains a large amount of evidence for the existence of normal faults.

Comparing the experimental results with the seismic profiles shows that the graben comprised normal faults that formed during D_1 (f_{12} and f_{14} in Fig. 16(h)) has the same geometry as the basement graben observed in actual seismic profiles (f_{47} and f_{48} in Fig. 16(c)), two normal faults with high and steep dips in opposite directions, developed in the middle of the Junggar Basin and the simulated

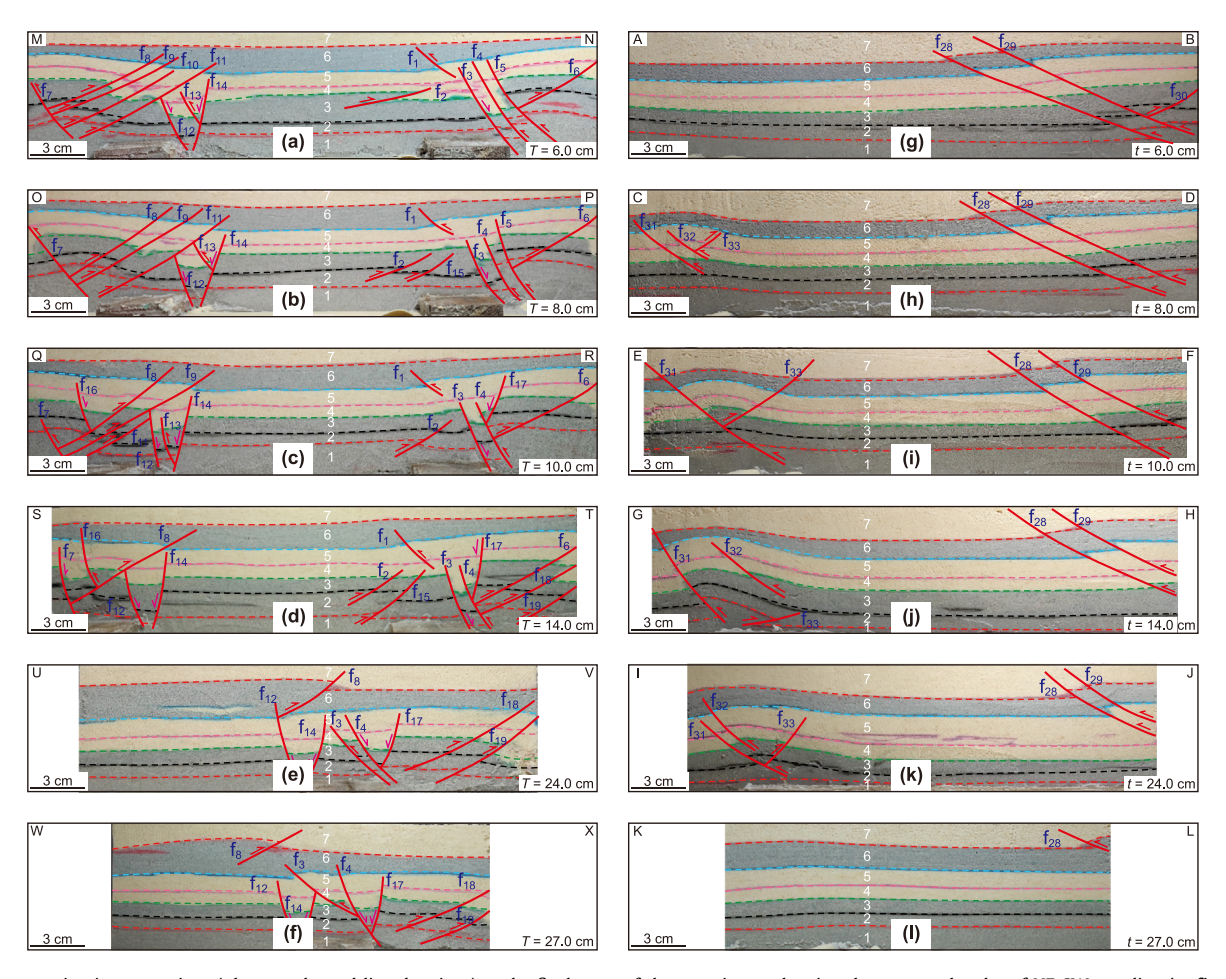


Fig. 14. Cross-section interpretations (photographs and line drawings) at the final stage of the experiment showing the structural styles of NE-SW trending (**a**–**f**) and NW-SE trending (**g**–**l**). "T" represents the distance from the cross-section to the boundary steel board in the direction of motor 3, "t" represents the distance from the cross-section to the boundary steel board in the direction of motor 1. See cross-section locations in Fig. 13(**h**).

experimental setup. In the D_3 compressional phase, the transpressional structures (f_7-f_{11} in Fig. 16(d), (e); f_7-f_9 and f_{16} in Fig. 16(f), (g)) formed by the basement faults due to the presence of strike-slip displacements are similar to the flower-like structures formed by the Triassic transpressional stress in the central basin seismic section (Fig. 16(a), (b)). The main fault maintains a normal fault throw at the bottom of the profile, and due to the influence of late tectonic movements, there is a certain degree of positive inversion in the middle layer position. A large number of small strike-slip faults have developed horizontally within the lower layer of the Jurassic system. These faults tend to converge relatively and concentrate towards the main fault on both sides, forming a positive flower structure characterized by downward convergence and upward divergence.

Comparison of the actual geological data shows that the simulation experiments conducted in this study are highly reliable and can accurately restore the tectonic evolution of early extensional superposition with late multi-phase non-coaxial compression in the Junggar Basin, providing strong support for the study of superposition deformation in the study area.

The relationship between multi-phase tectonic superposition and hydrocarbon accumulation has long been discussed in the field of petroleum geology (Hao et al., 2000, 2011; Yang and Liu, 2000; Cao et al., 2005). Multiple tectonic movements are also the reasons for the adjustment and destruction of early formed oil and gas reservoirs, as well as the formation of secondary oil and gas

reservoirs (Wang et al., 2018). The multi-phase tectonic evolution of sedimentary basins exerts a significant control on the distribution and accumulation of hydrocarbons. Through the interplay of various tectonic events over geological time scales, the structural architecture of sedimentary basins undergoes complex modifications, influencing the formation and preservation of hydrocarbon reservoirs. The sequential nature of tectonic events, including rifting, compression, and extension, creates diverse structural settings within sedimentary basins. These tectonic phases resulted in the development of fault systems, folds, and fractures, which served as primary conduits and traps for migrating hydrocarbons. For example, extensional tectonic movement may create faultbounded rift basins, facilitating the migration and accumulation of hydrocarbons along fault zones and structural highs. Also, the structural evolution of sedimentary basins influences the geometry and distribution of reservoir rocks, affecting the storage capacity and productivity of hydrocarbon accumulations. Differential subsidence and uplift associated with tectonic phases result in the formation of stratigraphic traps, anticlinal structures, and faultrelated traps, which control the spatial distribution of hydrocarbon reservoirs. Furthermore, the timing and duration of multiple tectonic events play a crucial role in determining the maturity and preservation of hydrocarbon accumulations. Early tectonic phases may create conducive conditions for hydrocarbon generation and migration, while later tectonic phases may modify reservoir properties and seal integrity. Taking Qaidam Basin in western China as

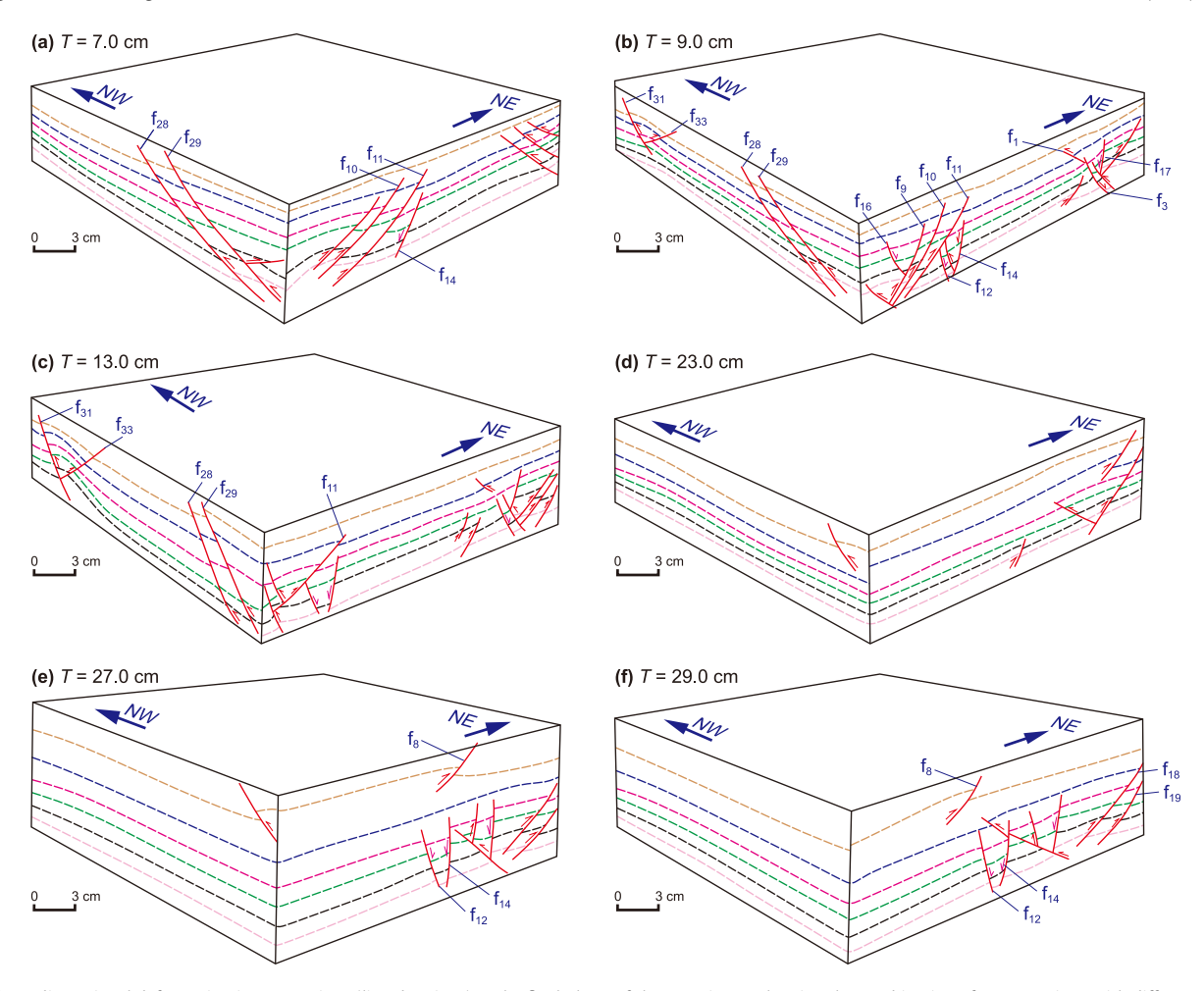


Fig. 15. Three-dimensional deformation interpretations (line drawings) at the final phase of the experiment showing the combination of cross-sections with different strikes. "T" represents the distance from the edge of the experimental apparatus on motor 1 side.

an example, there was a long-time interval between the Carboniferous passive continental margin and the Jurassic foreland basin sedimentation in the northern margin of Qaidam, and the average residual organic carbon mass fraction in carbonate rocks is 2.55%; Chloroform asphalt "A" has an average of 0.005% (Yang and Liu, 2000). Generally speaking, if the burial depth of the Carboniferous source rock is greater than 2800 m, it enters the stage of crude oil cracking. The Carboniferous system on the northern edge of Qaidam has been deeply buried under several prototype basins of the Mesozoic and Cenozoic eras, with a burial depth greater than 5000 m, and has entered an over mature stage. The passive continental margin of Tarim and the Junggar Basins is better than Qaidam Basin, Jiuquan Basin and other basins in hydrocarbon generation, because the passive continental margin deposition followed by foreland basin deposition is conducive to hydrocarbon generation and oil and gas preservation Therefore, a comprehensive understanding of the temporal sequence of tectonic events is essential for assessing the petroleum potential of sedimentary basins and predicting the distribution of hydrocarbon accumulations.

7. Conclusion

In this study, the geological structure and multi-phase tectonic evolution of the Junggar Basin were studied by field outcrop observation, seismic profiles geological interpretation, and sandbox analogue modelling. The study conclusions are as follows.

- (1) The tectonic evolution of the Junggar Basin since the Late Paleozoic can be divided into five main phases: the Late Carboniferous to Early Permian extensional and faulting phase, the Middle to Late Permian compression and thrust phase, the Triassic to Jurassic transpressional phase, the Cretaceous uniform subsidence stage, and the foreland compression phase since the Paleozoic. Multi-strike faults with different properties in different margins and middle of the basin stem from the composite superposition of multi-phase non-coaxial stress fields.
- (2) The strong spatial and temporal differences during the formation of the Junggar Basin due to the collision of the Kazakhstan plate, the Tarim plate, and the Siberian plate yielded complex composite superimposed structures. The Late Paleozoic Hercynian movement resulted in a relatively unified basement of the Junggar Basin, and the basin was controlled by different regional dynamics during the Indo-Chinese, Yanshan, and Himalayan phases of regional tectonic movements, which led to the development of multiphase sedimentary basins with different properties.
- (3) Due to the nearly triangular shape of the Junggar Basin, the Cenozoic thrusting from the northern Tianshan only occurred in the southern piedmont zone, while the northwestern, eastern, and central parts of the basin mostly retained the Mesozoic structural styles, affording different superimposed structural styles in each area.

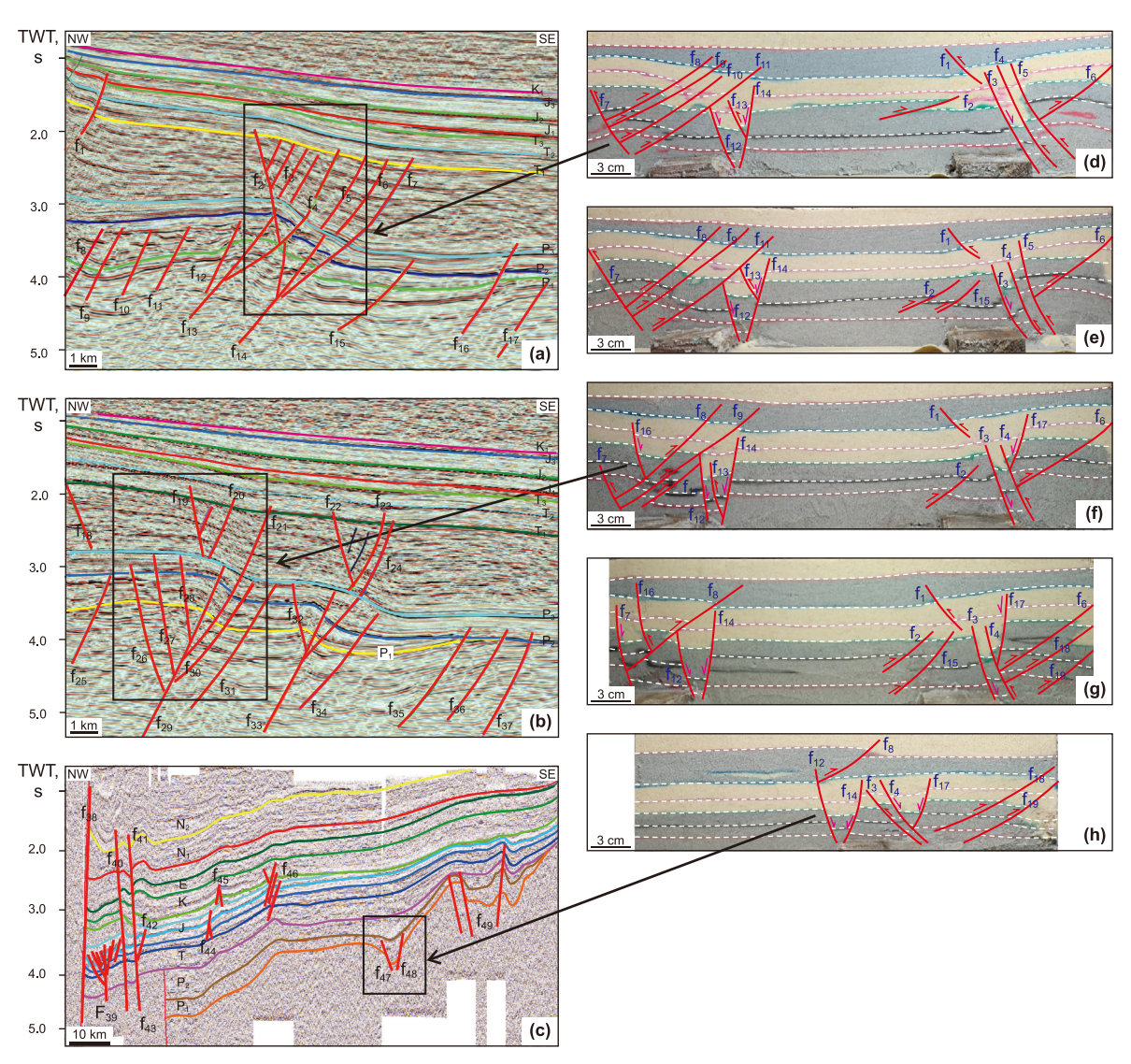


Fig. 16. Comparison between the analogue modelling result (d-h) and seismic interpretation result (a-c) of the Junggar Basin.

CRediT authorship contribution statement

Jing-Qi Zhang: Writing — review & editing, Writing — original draft, Investigation, Formal analysis, Data curation, Conceptualization. Fu-Sheng Yu: Supervision, Conceptualization. Yue-Feng Wang: Investigation, Formal analysis. Zhuo-Yi Shen: Resources, Data curation. Jin-Lei Xiu: Resources, Funding acquisition, Data curation. Yan Xue: Funding acquisition, Formal analysis. Long-Fei Shao: Software, Investigation.

Declaration of competing interest

The authors declare that they have no known competing financial interests or personal relationships that could have appeared to influence the work reported in this paper.

Acknowledgments

This study was supported by the National Natural Science Foundation of China, (Grant No. 42072144) and Shengli Oilfield, SINOPEC, China (Nos. 30200018-21-ZC0613-0030 and 30200018-20-ZC0613-0116). The authors gratefully acknowledge the editors

and three anonymous reviewers for their constructive comments and suggestions, which greatly improved the manuscript.

References

Bellahsen, N., Faccenna, C., Funiciello, F., Daniel, J.M., Jolivet, L., 2003. Why did Arabia separate from Africa? Insights from 3-D laboratory experiments. Earth Planet Sci. Lett. 216 (3), 365–381. https://doi.org/10.1016/S0012-821X(03) 00516-8.

Bonini, M., Sokoutis, D., Talbot, C.J., Boccaletti, M., Milnes, A.G., 1999. Indenter growth in analogue models of Alpine-type deformation. Tectonics 18 (1), 119–128. https://doi.org/10.1029/1998TC900008.

Brace, W.F., Kohlstedt, D.L., 1980. Limits on lithospheric stress imposed by laboratory experiments. J. Geophys. Res. Solid Earth 85 (B11), 48–52. https://doi.org/10.1029/JB085iB11p06248.

Buchanan, P.G., McClay, K.R., 1991. Sandbox experiments of inverted listric and planar fault systems. Tectonophysics 188 (1), 97–115. https://doi.org/10.1016/0040-1951(91)90317-L.

Chen, S.P., Zhang, Y.W., Tang, L.J., 2001. Evolution of Junggar late carboniferouspermian foreland basin. J. Univ. Pet., China (Ed. Soc. Sci.) 25 (5), 11–15+23 (in Chinese).

Chen, X., Lu, H.F., Shu, L.S., Wang, H.M., Zhang, G.Q., 2002. Study on tectonic evolution of Junggar Basin. Geol. J. China Univ. 8 (3), 257–267 (in Chinese).

Cao, J., Zhang, Y.J., Hu, W.X., Yao, S.P., Wang, X.L., Zhang, Y.Q., Tang, Y., 2005. The Permian hybrid petroleum system in the northwest margin of the Junggar Basin, northwest China. Mar. Petrol. Geol. 22 (3), 331–349. https://doi.org/ 10.1016/j.marpetgeo.2005.01.005.

Colletta, B., Letouzey, J., Pinedo, R., Ballard, J.F., Balé, P., 1991. Computerized X-ray tomography analysis of sandbox models: examples of thin-skinned thrust systems. Geology 19 (11), 1063–1067. https://doi.org/10.1130/0091-7613(1991) 019

- Costa, E., Vendeville, B.C., 2002. Experimental insights on the geometry and kinematics of fold-and-thrust belts above weak, viscous evaporitic décollement. J. Struct. Geol. 24 (11), 1729–1739. https://doi.org/10.1016/S0191-8141(01)
- Davy, P., Cobbold, P.R., 1991. Experiments on shortening of a 4-layer model of the continental lithosphere. Tectonophysics 188, 1–25. https://doi.org/10.1016/ 0040-1951(91)90311-F.
- Ding, W.L., Jin, Z.J., Zhang, Y.J., Zeng, J.H., Wang, H.Y., 2011. Experimental simulation of faults controlling oil migration and accumulation in the central part of Junggar basin and its significance for petroleum geology. Earth Sci. 36 (1), 73–82. https://doi.org/10.3799/dqkx.2011.008 (in Chinese).
- Dooley, T.P., Schreurs, G., 2012. Analogue modelling of intraplate strike-slip tectonics: a review and new experimental results. Tectonophysics 574–575, 1–71. https://doi.org/10.1016/j.tecto.2012.05.030.
- Fang, S.H., Jia, C.Z., Guo, S.J., Song, Y., Xu, H.M., Liu, L.J., 2006. New view on the Permian evolution of the Junggar basin and its implications for tectonic evolution. Earth Sci. Front. 13 (3), 108–121 (in Chinese).
- Hao, F., Zhang, Z.H., Zou, H.Y., Zhang, Y.C., Yang, Y.Y., 2011. Origin and mechanism of the formation of the low-oil-saturation Moxizhuang field, Junggar Basin, China: implication for petroleum exploration in basins having complex histories. AAPG (Am. Assoc. Pet. Geol.) Bull. 95 (6), 983–1008. https://doi.org/10.1306/11191010114.
- Hao, F., Zou, H.Y., Jiang, J.Q., 2000. Dynamics of petroleum accumulation and its advances. Earth Sci. Front. 7 (3), 11–21 (in Chinese).
- He, D.F., 2022. Multi-cycle superimposed sedimentary basins in China: formation, evolution, geologic framework and hydrocarbon occurrence. Earth Sci. Front. 29 (6), 24–59. https://doi.org/10.13745/j.esf.sf.2022.8.1 (in Chinese).
- He, D.F., Li, D., Tong, X.G., Zhao, W.Z., 2008. Accumulation and distribution of oil and gas controlled by paleo-uplift in poly-history superimposed basin. Acta Pet. Sin. 29 (4), 475–488. https://doi.org/10.7623/syxb200804001 (in Chinese).
- He, D.F., Li, D.S., Tong, X.G., 2010. Stereoscopic exploration model for multi-cycle superimposed basins in China. Acta Pet. Sin. 31 (5), 695–709. https://doi.org/10.7623/syxb201005001 (in Chinese).
- He, D.F., Ma, Y.S., Liu, B., Cai, X.Y., Zhang, Y.J., Zhang, J., 2019. Main advances and key issues for deep-seated exploration in petroliferous basins in China. Earth Sci. Front. 26 (1), 1–12. https://doi.org/10.13745/j.esf.sf.2019.1.20 (in Chinese).
- He, D.F., Zhang, L., Wu, S., Li, D., Zhen, Y., 2018. Tectonic evolution stages and features of the Junggar Basin. Oil Gas Geol. 39 (5), 845–861. https://doi.org/10.11743/ogg20180501 (in Chinese).
- Hu, S.Y., Wang, X.J., Cao, Z.L., Li, J.Z., Gong, D.Y., Xu, Y., 2020. Formation conditions and exploration direction of large and medium gas reservoirs in the Junggar Basin, NW China. Petrol. Explor. Dev. 47 (2), 247–259. https://doi.org/10.11698/ PED.2020.02.04 (in Chinese).
- Hubbert, M.K., 1937. Theory of scale models as applied to the study of geologic structures. Geol. Soc. Am. Bull. 48, 1459–1520. https://doi.org/10.1130/GSAB-48.1450
- Koyi, H.A., 1997. Analogue modelling: from a qualitative to a quantitative technique—a historical outline. J. Petrol. Geol. 20 (2), 223–238. https://doi.org/10.1111/j.1747-5457.1997.tb00774.x.
- Koyi, H.A., Kenneth, P., 1993. Influence of basement faults on the development of salt structures in the Danish Basin. Mar. Petrol. Geol. 10 (2), 82–94. https:// doi.org/10.1016/0264-8172(93)90015-K.
- Koyi, H.A., Vendeville, B.C., 2003. The effect of décollement dip on geometry and kinematics of model accretionary wedges. J. Struct. Geol. 25 (9), 45–50. https:// doi.org/10.1016/S0191-8141(02)00202-X.
- Lai, S.X., Huang, K., Chen, J.L., Wu, J., Qian, W.C., Chen, S.P., Xu, H.M., 1999. Evolution and oil/gas accumulation of late carboniferous and Permian foreland basin in Junggar Basin. Xinjing Pet. Geol. 20 (4), 293–297 (in Chinese).
- Li, D., He, D.F., Santosh, M., Ma, D.L., 2015. Tectonic framework of the northern Junggar Basin part II: the island arc basin system of the western Luliang Uplift and its link with the West Junggar terrane. Gondwana Res. 27 (3), 1110–1130. https://doi.org/10.1016/j.gr.2014.08.019.
- McClay, K.R., 1990. Extensional fault systems in sedimentary basins: a review of analogue model studies. Mar. Petrol. Geol. 7 (3), 206–233. https://doi.org/ 10.1016/0264-8172(90)90001-W.
- McClay, K.R., Buchanan, P., 1992. Thrust faults in inverted extensional basins. In: McClay, K.R. (Ed.), Thrust Tectonics. Springer, Dordrecht, pp. 93–104. https://doi.org/10.1007/978-94-011-3066-0_8.
- Moore, V.M., Vendeville, B.C., Wiltschko, D.V., 2005. Effects of buoyancy and mechanical layering on collisional deformation of continental lithosphere: results from physical modeling. Tectonophysics 403 (1–4), 193–222. https://doi.org/10.1016/j.tecto.2005.04.004.
- Pang, X.Q., 2010. Key challenges and research methods of petroleum exploration in the deep of superimposed basins in western China. Oil Gas Geol. 31 (5), 517–534+541. https://doi.org/10.11743/ogg20100501 (in Chinese).
- Persson, K.S., Sokoutis, D., 2002. Analogue models of orogenic wedges controlled by erosion. Tectonophysics 356 (4), 323–336. https://doi.org/10.1016/S0040-1951(02)00443-2.
- Qu, G.S., Ma, Z.J., Chen, X.F., Li, T., Zhang, N., 2009. On structure and evolution in

- Junggar Basin, Xinjing Pet. Geol. 30 (1), 1–5 (in Chinese).
- Rahe, B., Ferrill, D.A., Morris, A.P., 1998. Physical analog modeling of pull-apart basin evolution. Tectonophysics 285 (1–2), 21–40. https://doi.org/10.1016/S0040-1951(97)00193-5.
- Ramsay, J.G., 1962. Interference patterns produced by the superposition of folds of similar type. J. Geol. 71, 466–481.
- Ramsay, J.G., Huber, M.I., 1987. The Techniques of Modern Structural Geology, vol. 2. folds and fractures, Academic press, Massachusetts.
- Rao, S., Zhu, Y.K., Hu, D., Hu, S.B., Wang, Q., 2018. The thermal history of Junggar Basin: constraints on the tectonic attribute of the Early-middle Permian basin. Acta Geol. Sin. 92 (6), 1176–1195 (in Chinese).
- Reynolds, D.L., Holmes, A., 1954. The superposition of Caledonoid folds on an older fold-system in the Dalradians of Malin Head, Co. Donegal. Geol. Mag. 91 (6), 417–444. https://doi.org/10.1017/S0016756800066267.
- Rossetti, F., Faccenna, C., Ranalli, G., Storti, F., 2000. Convergence rate-dependent growth of experimental viscous orogenic wedges. Earth Planet Sci. Lett. 178 (3–4), 367–372. https://doi.org/10.1016/S0012-821X(00)00082-0.
- Shen, Z.Y., Yu, F.S., Wang, Q.J., Zhang, J.Q., Xue, Y., 2022. Discrete element method simulation of the fold-and-thrust belts along strike various compression in the southern margin of the Junggar Basin, China. Mar. Petrol. Geol. 145, 105849. https://doi.org/10.1016/j.marpetgeo.2022.105849.
 Song, L.H., Zhu, G., Gu, C.C., Zhai, M.J., 2015. Orogeny-related activities of Kalamaili
- Song, L.H., Zhu, G., Gu, C.C., Zhai, M.J., 2015. Orogeny-related activities of Kalamaili Fault Zone and their indications to the orogenic processes. Geol. Rev. 61 (1), 79–94 (in Chinese).
- Wang, H.H., Wu, K.Y., Pei, Y.W., Guo, W.J., Liu, B., 2015. Thrust/Strike-slip-fault belt structures evolution characteristics and physical modeling of Zaire Mountain. J. Geomechanics 21 (2), 56–65 (in Chinese).
- Wang, X.J., Song, Y., Zheng, M.L., Ren, H.J., Wu, H.S., He, W.J., Wang, T., Wang, X.T., Zhao, C.Y., Guo, J.C., 2021. Composite petroleum system and multi-stage hydrocarbon accumulation in Junggar Basin. China Petroleum Exploration 26 (4), 29–43. https://doi.org/10.3969/j.issn.1672-7703.2021.04.003 (in Chinese).
- Wang, X.J., Song, Y., Zheng, M.L., Guo, X.G., Wu, H.S., Ren, H.J., Wang, T., Chang, Q.S., He, W.J., Wang, X.T., Guo, J.C., Huo, J.J., 2022. Tectonic evolution of and hydrocarbon accumulation in the west Junggar Basin. Earth Sci. Front. 29 (6), 188–205. https://doi.org/10.13745/j.esf.sf.2022.8.19.
- Wang, Y.J., Jia, D., Pan, J.G., Wei, D.T., Tang, Y., Wang, G.D., Wei, C.R., Ma, D.L., 2018. Multiple-phase tectonic superposition and reworking in the Junggar Basin of northwestern China—implications for deep-seated petroleum exploration. AAPG (Am. Assoc. Pet. Geol.) Bull. 102 (8), 1489—1521. https://doi.org/10.1306/ 10181716518.
- Wang, Y.X., Hou, G.T., Liu, S.L., Li, L., Niu, X.L., Xiao, F.F., 2011. Numerical simulation of tectonic dynamics of the Junggar basin at the end of Paleozoic. Chin. J. Geophys. 54 (2), 441–448. https://doi.org/10.3969/j.issn.0001-5733.2011.02.022 (in Chinese).
- Weijermars, R., Schmeling, H., 1986. Scaling of Newtonian and non-Newtonian Fluid dynamics without inertia for quantitative modelling of rock flow due to gravity (including the concept of rheological similarity). Phys. Earth Planet. In. 43 (4), 316–330. https://doi.org/10.1016/0031-9201(86)90021-X.
- Wu, K.Y., Zha, M., Wang, X.L., Qu, J.X., Chen, X., 2005. Further researches on the tectonic evolution and dynamic setting of the Junggar Basin. Acta Geosci. Sin. (3), 217–222. https://doi.org/10.3321/j.issn:1006-3021.2005.03.004 (in Chinese).
- Xiao, X.C., Tang, Y.Q., Feng, Y.M., Zhu, B.Q., Li, J.Y., Zhao, M., 1992. Tectonics in Northern Xinjiang and its Adjacent Areas. Geology Press, Beijing.
- Yan, D.P., Xu, Y.B., Dong, Z.B., Qiu, L., Zhang, S., Wells, M., 2016. Fault-related fold styles and progressions in fold-thrust belts: insights from sandbox modeling. J. Geophys. Res. Solid Earth 121 (3), 2087–2111. https://doi.org/10.1002/ 2015IB012397.
- Yang, W.L., Wang, Y., Li, Y.H., Li, Y.H., 2003. Simulation of structural stress field during yanshan movement in Junggar Basin. Xinjing Pet. Geol. 24 (2), 124–126 (in Chinese).
- Yang, M.H., Liu, C.Y., 2000. Characters of Quasi-Foreland basins in western-central China and their oil and gas potential. Oil Gas Geol. 21 (1), 46–49 (in Chinese).
- Yu, F.S., Koyi, H.A., 2016. Cenozoic tectonic model of the bohai bay Basin in China. Geol. Mag. 153 (5–6), 866–886. https://doi.org/10.1017/S0016756816000492.
- Yu, F.S., Koyi, H.A., 2017. Theoretical and experimental estimation of geometric relationship of non-parallel conjugate normal faults. Tectonophysics 703, 85–97. https://doi.org/10.1016/j.tecto.2017.03.009.
- Yu, F.S., Li, G.Z., Yang, G.D., Ma, B.J., Chen, S.P., 2009. Deformation feature and genesis simulation of fold-and-thrust belts in the southern margin, Junggar Basin. Geotect. Metallogenia 33 (3), 386–395 (in Chinese).
- Yu, F.S., Zhang, R.F., Yu, J.F., Wang, Y.D., Chen, S.G., Liu, J., Wu, C.L., Wang, Y.Q., Wang, S.C., Wang, Y.H., Liu, Y.L., 2021. Meso-cenozoic negative inversion model for the linhe depression of hetao basin, China. Geol. Mag. 159 (4), 535–560. https://doi.org/10.1017/S0016756821001138.
- Zhang, G.C., Liu, L.J., Chen, X.F., Liu, J.W., 1998. Structure and trap types of Junggar Basin. Xinjiang Geol. 16 (3), 221–230 (in Chinese).
- Zhang, X.C., Ma, D.L., Wei, L.Y., Wang, H.B., Wang, Y.J., Liu, W.Q., Yang, X.L., 2020. Deformation mechanism of Hutubi anticline in the southern margin of Junggar Basin: insights from physical simulation experiment. Xinjing Pet. Geol. 41 (zk1), 92–100. https://doi.org/10.7657/XJPG20200115 (in Chinese).
- Zhang, J.Q., Yu, F.S., Pang, F.J., Wang, Q.J., Wang, Y.F., 2024. Development characteristics and analogue modelling of strike-slip faults in the Yongjin area, central

Junggar basin. Acta Geol. Sin. 98 (2), 397–420. https://doi.org/10.19762/j.cnki.dizhixuebao.2023151 (in Chinese).
Zhao, B., 1992. Formation and evolution of Junggar Basin. Xinjing Pet. Geol. 13 (3), 191–196 (in Chinese).

Zhou, J.X., 1999. Sandbox experimental modeling on the inversion tectonics of half-

graben. Prog. Geophys. 14 (3), 47–52 (in Chinese).

Zhou, P.X., Wu, K.Y., Dong, F., Li, Y.Y., 2023. Denudation thickness and distribution rule in the fault-depression transition period of Junggar Basin. Geol. Resour. 32 (5), 575–583. https://doi.org/10.13686/j.cnki.dzyzy.2023.05.007 (in Chinese).